JCI The Journal of Clinical Investigation

GMPPA defects cause a neuromuscular disorder with α-dystroglycan hyperglycosylation

Patricia Franzka, … , Julia von Maltzahn, Christian A. Hübner

J Clin Invest. 2021. https://doi.org/10.1172/JCI139076.

Research In-Press Preview **Muscle biology**

Graphical abstract

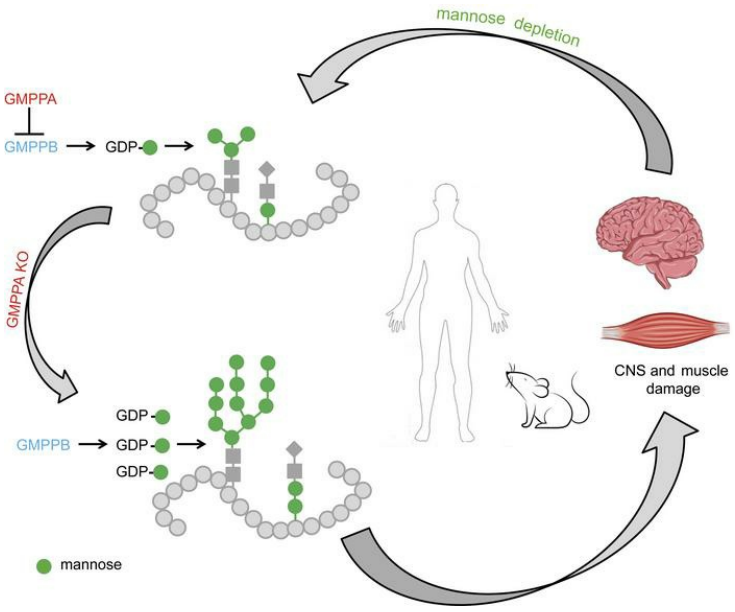

GMPPA defects cause a neuromuscular disorder with α-dystroglycan hyperglycosylation

Authors: Patricia Franzka[1], Henriette Henze[2]†, M. Juliane Jung[2]†, Svenja Caren Schüler[2], Sonnhild Mittag[3], Karina Biskup[4], Lutz Liebmann[1], Takfarinas Kentache[5], José Morales[6], Braulio Martínez[7], Istvan Katona[8], Tanja Herrmann[1], Antje-Kathrin Huebner[1], J. Christopher Hennings[1], Susann Groth[2], Lennart Gresing[1], Rüdiger Horstkorte[8], Thorsten Marquardt[9], Joachim Weis[8], Christoph Kaether[2], Osvaldo M. Mutchinick[6], Alessandro Ori[2], Otmar Huber[3], Veronique Blanchard[4], Julia von Maltzahn[2], Christian A. Hübner[1]*

Affiliations:

[1]Institute of Human Genetics, University Hospital Jena, Friedrich Schiller University, Jena, Germany
[2]Leibniz-Institute on Aging - Fritz-Lipmann-Institute, Jena, Germany
[3]Department of Biochemistry II, University Hospital Jena, Friedrich Schiller University, Jena, Germany
[4]Charité-Universitätsmedizin Berlin, corporate member of Freie Universität Berlin, Humboldt-Universität zu Berlin, and Berlin Institute of Health, Institute of Laboratory Medicine, Clinical Chemistry and Pathobiochemistry, Berlin, Germany
[5]Welbio and de Duve Institute, Université Catholique de Louvain, Brussels, Belgium
[6]Department of Genetics, Instituto Nacional de Ciencias Médicas y Nutrición "Salvador Zubirán", Mexico City, Mexico
[7]Department of Pathology, Instituto Nacional de Ciencias Médicas y Nutrición "Salvador Zubirán", Mexico City, Mexico
[8]Institut für Neuropathologie, Institute of Neuropathology, RWTH Aachen University Hospital, Aachen, Germany
[8]Institut für Physiologische Chemie, Martin-Luther-Universität Halle-Wittenberg, Halle, Germany
[9]University Hospital Muenster, Department of Pediatrics, Muenster, Germany

† equal contribution

* corresponding author: christian.huebner@med.uni-jena.de

University Hospital Jena, Am Klinikum 1, 07747 Jena, Germany

Phone 0049-3641-9396800, Fax 0049-3641-9396802

Declaration of Interests

The authors declare no competing interests.

Abstract:

GDP-mannose-pyrophosphorylase-B (GMPPB) facilitates the generation of GDP-mannose, a sugar donor required for glycosylation. GMPPB defects cause muscle disease due to hypoglycosylation of α-dystroglycan (α-DG). Alpha-DG is part of a protein complex, which links the extracellular matrix with the cytoskeleton thus stabilizing myofibers. Mutations of the catalytically inactive homolog GMPPA cause AAMR syndrome, which is characterized by achalasia, alacrima, mental retardation, and muscle weakness. Here we show that *Gmppa* KO mice recapitulate cognitive and motor deficits. As structural correlates we found cortical layering defects, progressive neuron loss, and myopathic alterations. Increased GDP-mannose levels in skeletal muscle and in vitro assays identify GMPPA as an allosteric feedback inhibitor of GMPPB. Thus, its disruption enhances mannose incorporation into glycoproteins including α-Dg in mice and men. This increases α-Dg turnover and thereby lowers α-Dg abundance. In mice dietary mannose restriction beginning after weaning corrects α-DG hyperglycosylation and abundance, normalizes skeletal muscle morphology, and prevents neuron degeneration and the development of motor deficits. Cortical layering and cognitive performance, however, are not improved. We thus identify GMPPA defects as the first congenital disorder of glycosylation characterized by α-DG hyperglycosylation, unravel underlying disease mechanisms and point to potential dietary treatment options.

Introduction

Cell surface proteins are important for the attachment of a cell to the extracellular matrix (ECM). They are modified by post-translational covalent attachment of branched carbohydrate oligomers. While *N*-linked oligosaccharides are linked to asparagine, *O*-linked glycans are mainly attached to serine, threonine or tyrosine. The process of glycosylation starts at the endoplasmic reticulum (ER) and proceeds in the Golgi apparatus. Abnormal glycosylation of proteins can induce deleterious effects as observed in congenital disorders of glycosylation (CDG), which often result in serious, sometimes fatal malfunctions of different organ systems such as brain and muscle (1). One example are mutations in the gene encoding GDP-mannose-pyrophosphorylase-B (GMPPB), which result in variable skeletal muscle disorders including muscular dystrophy and myasthenia (2-5), which are characterized by hypoglycosylation of the sarcolemma-associated protein α-dystroglycan (α-DG). GMPPB catalyzes the production of GDP-mannose from mannose-1-phosphate and GTP (6), which is required as a sugar donor for glycosylation of proteins. We recently identified mutations in the gene encoding GDP-mannose-pyrophosphorylase-A (GMPPA) in patients suffering from a clinically variable syndrome characterized by symptoms such as muscle weakness, muscular hypotonia, gait abnormalities, problems to swallow (achalasia), reduced or absent tear flow (alacrima) and mental retardation, which is also known as AAMR syndrome (7). Whether GMPPA plays a role in the glycosylation of α-DG remained unclear, because GMPPA is catalytically inactive (6).

Alpha-DG is a highly glycosylated extracellular peripheral membrane protein non-covalently attached to the transmembrane protein β-dystroglycan (β-DG). Both proteins are encoded by a single gene (*DAG1*) and are generated by cleavage of a common precursor. Alpha-DG binds to ECM components such as laminin via its glycan side chains, while β-DG is connected to cytoplasmic proteins including dystrophin. These proteins are part of the dystroglycan complex (DGC), which acts as a linker between the ECM and the intracellular cytoskeleton thereby

stabilizing myofibers (8, 9). Mutations in different members of the DGC lead to muscular dystrophy in mice and men and affect both myofibers and muscle stem cells (10). Glycosylation is the crucial modification that modulates the function of α-DG as a receptor for extracellular binding partners. Accordingly, hypoglycosylation of α-DG is a central event in the pathogenesis of several complex muscle disorders such as the Walker-Warburg-syndrome, which also affects the brain (11).

We here show that binding of GMPPA to GMPPB inhibits the activity of recombinant GMPPB in a GDP-mannose dependent manner, suggesting that GMPPA acts as an allosteric feedback inhibitor of GMPPB. *Gmppa* knockout (KO) mice show cognitive and motor impairment with progressive neuron loss and myopathic alterations. In agreement with a role as allosteric inhibitor of GMPPB, GDP-mannose levels are increased in skeletal muscle of *Gmppa* KO mice and lead to α-DG hyperglycosylation. Knockdown studies in myoblasts further reveal that the turnover of hyperglycosylated α-DG is increased thus leading to a reduced α-DG abundance. A myopathic disorder characterized by α-DG hyperglycosylation and decreased overall α-DG abundance is also evident in skeletal muscle biopsies of AAMR patients. In mice, α-DG hyperglycosylation, neuron loss, muscle damage and motor deficits can be prevented by a mannose-free diet starting at postnatal day (P) 14.

Results

Gmppa KO mice show progressive motor deficits and cognitive impairments

To study GMPPA deficiency we generated a *Gmppa* KO mouse model from targeted ES cell clones obtained from EUCOMM (EPD0621_7_G03) (**Figure 1A**). Chimeric mice were verified by Southern blot (**Supplementary Figure 1A)** and subsequently mated with FLPe- (12) and Cre-deleter mice (13). Mating of offspring with a heterozygous deletion of exon 5 resulted in the generation of homozygous mice at the expected Mendelian ratio. The predicted aberrant transcript devoid of exon 5 is predicted to lead to a frameshift and a premature termination of protein translation. *Gmppa* transcript abundance was drastically decreased in KO mice suggesting that the aberrant transcript undergoes nonsense-mediated decay (**Supplementary Figure 1B**). Immunoblot analysis for GMPPA detected bands of the expected size in different tissues from wild-type (WT) mice, which were absent in lysates of mice with a homozygous deletion of exon 5 (**Figure 1B**), further validating the successful knockout of GMPPA.

The bodyweight of young *Gmppa* KO mice (3 months of age) was indistinguishable from WT littermates while a significant decrease was observed at 12 months of age (**Supplementary Figure 1C,D**). To address whether KO mice develop gait abnormalities, as reported for many AAMR patients (7), we performed a beam-walk test (14). The foot-base-angle of the hind paw at toe-off-position was reduced in KO mice at 3 months of age and further flattened over time (**Figure 1C**), suggesting a progressive muscle weakness. Progressive muscle weakness was also evident for the forelimbs in the weights test (**Figure 1D**). Moreover, aged KO mice fell off a wire mesh more rapidly than control littermates (**Figure 1E**).

To assess cognitive function, we performed a contextual and cued fear conditioning test with 3- and 12-month-old WT and KO mice (**Figure 1F**), which tests the ability of KO mice to learn and remember an association between environmental cues and averse experiences. Freezing behavior during the test was measured as an index of fear memory. For acquisition, mice were placed into a conditioning chamber and were given pairings of the conditioned auditory stimulus (the auditory cue) and an electric foot-shock. After 24 h, mice were either exposed to

a different chamber with presentation of the auditory cue (cued test) or the same context as for acquisition (context test). While both WT and KO mice learned the conditioned stimulus, KO mice were unable to remember the context of the aversive stimulus, which suggests a defect in hippocampus dependent learning in *Gmppa* KO mice (15).

Taken together, *Gmppa* KO mice reproduce cognitive and motor impairments as reported for AAMR patients.

Gmppa disruption in mice affects brain development and long-term neuronal maintenance

The histological analysis of the somatosensory cortex revealed that the layering of the neocortex is altered in young *Gmppa* KO mice (**Figure 2A**). Apart from this developmental defect, we also observed an age-dependent loss of hippocampal pyramidal neurons (**Figure 2B**) and Purkinje cells (**Figure 2C**).

We also analyzed the peripheral nervous system. Sciatic nerve fiber numbers at 12 months of age did not differ between genotypes and the distribution of axon diameters was normal (**Figure 2D**). In agreement, compound muscle action potentials (CMAPs) at the tail tip in response to electrical stimulation at the root of the tail and the efferent nerve conduction velocity were not altered in 12-month-old KO mice (**Figure 2E**). While the sensory amplitudes were unaffected, we noted a mild decrease of the sensory velocity in 12-month-old KO mice (**Figure 2F**).

These data show that loss of GMPPA entails both neurodevelopmental as well as neurodegenerative components, which mainly manifest in the central nervous system.

Gmppa KO mice develop an age-dependent myopathy

Consistent with progressive motor impairments and decreased muscle strength, the mass of the M. tibialis anterior, the M. gastrocnemius together with M. soleus, and the M. palmaris longus was lower in 12-month-old KO mice (**Figure 3A**). Serum levels of creatinine kinase as a sign of pronounced muscle damage were not increased at 3 (**Supplementary Figure 2A**)

and 12 months of age (data not shown). A decrease of the mean myofiber diameter and an increased number of centrally located nuclei in musculus tibialis anterior sections was evident at 12 months of age (**Figure 3B**). A myofiber type-specific analysis is shown for the M. gastrocnemius/soleus in Supplementary Figure 6. Of note, we did not observe grouped degenerating myofibers as a typical sign of neurogenic muscle degeneration. TUNEL staining revealed a significant increase in apoptotic myofibers in KO samples (**Figure 3C**). Picro Sirius red stainings excluded a relevant fibrosis of skeletal muscles in *Gmppa* KO mice as often observed in muscular dystrophies (**Figure 3D**). We did not observe changes in the oxidative potential as judged from NADH-diaphorase staining (**Supplementary Figure 2B**). Staining for developmental myosin heavy chain (dev. MHC), a marker for regenerating myofibers, suggested that muscle regeneration is increased (**Figure 3E**).

Since the ECM serves as the interface between myofibers and the external environment and plays an active role in developmental and regenerative processes, we analyzed the localization of typical ECM proteins such as laminin, nidogen, and collagen IV. Laminin showed a more fragmented localization in skeletal muscles from KO mice at 12 months of age (**Figure 3F** and **Supplementary Figure 2C**), which was not yet evident at 3 months (data not shown). Similar findings were also observed for nidogen (**Figure3G** and **Supplementary Figure 2D**) and collagen IV (**Figure 3H** and **Supplementary Figure 2E**). Control stainings of WT and KO skeletal muscle sections with the respective secondary antibodies omitting primary antibodies did not show significant background staining (**Supplementary Figure 2F**). The sarcolemma was still intact in 12-month-old KO mice as judged by IgG stainings (**Supplementary Figure 2F**). Electron micrographs, however, suggest that the connection between myofiber basal lamina and endomysial collagen is less compact and tight in KO samples (**Figure 3I**). Overall protein abundances of laminin, nidogen and collagen IV were not altered as measured by immunoblot analyses of skeletal muscle lysates (**Supplementary Figure 2H**).

Mass spectrometry of skeletal muscle lysates identified proteins related to muscle contraction such as the Z-disc related protein CAPZB as significantly decreased in KO samples (**Figure 3J**, **Supplementary Figure 2I** and **Supplementary Table 1**). Because of these data, we

performed immunofluorescence stainings for α-actinin, a member of the spectrin family, which anchors myofibrillar actin filaments to Z-discs. Although being quite unspecific for myopathic disorders, staining for α-actinin was less intense and lacked the regular pattern in KO mice at 12 months of age (**Figure 3K**). Patches with myofibrillar disintegration and Z band streaming in KO samples were also evident by electron microscopy (**Figure 3L**).

In summary, *Gmppa* KO mice develop a progressive muscle disease.

GMPPA is an allosteric feedback inhibitor of GMPPB

We reported that GDP-mannose levels were elevated in lymphoblastoid cells of AAMR patients (7). A significant increase in GDP-mannose levels was also evident in skeletal muscle of *Gmppa* KO mice (**Figure 4A**). This, in combination with the fact that GMPPA is enzymatically inactive but can bind GDP-mannose (16), lead us to the hypothesis that GMPPA may act as an allosteric feedback inhibitor of GMPPB and accordingly should interact with GMPPB. To further evaluate this assumption, HEK-293T cells were transiently transfected with Myc-tagged GMPPA and FLAG-tagged GMPPB and subsequently protein complexes were immunoprecipitated from cell lysates. Co-precipitation of GMPPA with GMPPB and vice versa was detectable (**Figure 4B,C**). Notably, the disease-associated GMPPA variant p.T334P, located C-terminal of the nucleotidyl transferase domain, did no co-precipitate with GMPPB (**Figure 4C**). The interaction was preserved for the variant p.G182D, which locates to the nucleotidyl transferase domain. Because GMPPA variants devoid of the C-terminal 205 amino acids did not co-precipitate with GMPPB (**Figure 4D**), these findings suggest that the interaction requires the intact C-terminal part of GMPPA. Purified recombinant GST-GMPPB pulled down MBP-GMPPA only in the presence of the C-terminal part of GMPPA (**Figure 4E,F** and **Supplementary Figure 3A**), which points to a direct interaction between both proteins. Pull-down assays further suggest that the binding of the p.G182D and even more of the p.T334P variant of GMPPA to GMPPB is reduced.

The interaction between both WT proteins could be further substantiated by proximity ligation assays (PLA) on murine skeletal muscle sections with antibodies directed against GMPPA and

GMPPB. Only in cross sections of WT skeletal muscle the PLA-signal was detected, which indicates proximity of the targets of less than 40 nm (**Figure 4G** and **Supplementary Figure 3B,C**).

We also measured the GDP-mannose-pyrophosphorylase-activity of recombinant GMPPA and GMPPB by colorimetric readout of generated phosphate in the presence of mannose-1-phosphate, GDP-mannose, GTP, and pyrophosphatase (17). GMPPA alone was enzymatically inactive, but inhibited the activity of GMPPB (**Figure 4H** and **Supplementary Figure 3D-G**). This inhibition was preserved for the variant lacking the N-terminal part of GMPPA and absent for the variant lacking its C-terminal part (**Figure 4H**). Moreover, the inhibition of GMPPB by GMPPA depended on GDP-mannose concentration (**Figure 4I**). Notably, recombinant GMPPA N182D or T334P had no effect on the activity of GMPPB (**Figure 4J,K**).

Taken together our data suggest that GMPPA acts as an allosteric feedback inhibitor of GMPPB.

Alpha-DG is hyperglycosylated in skeletal muscle of *Gmppa* KO mice

The increase in GDP-mannose levels might cause imbalances in glycosylation reactions in *Gmppa* KO mice. We used mass spectrometry to identify alterations in the carbohydrate chains of either *N*-glycans or *O*-glycans of skeletal muscle. We found a significant increase in high-mannose *N*-glycans (**Figure 5A**) and in selected *O*-glycans (**Figure 5B**) in KO compared to control mice. Therefore, we separated skeletal muscle proteins from 12-month-old mice by SDS-PAGE and probed the blotted proteins with lectins such as concanavalin A (Con A) and peanut agglutinin (PNA) (**Figure 5C**), which bind to particular sugar sequences of glycoproteins. No obvious difference between genotypes was observed for Con A, which detects α-linked mannose, glucose or *N*-acetylgalactosamine. In contrast, signals for PNA, which detects non-sialylated β(1-3)-linked galactose on *N*-actelygalactosamine residues, were significantly increased in KO samples. The membranes were also probed with antibodies directed against oligomannose and paucimannose. Both were significantly increased in KO

lysates as well (**Figure 5C**). Because of our glycome analysis and the fact that α-DG is heavily glycosylated and its correct glycosylation is a prerequisite for muscle integrity (18, 19), we also assessed α-DG glycosylation. Indeed, we found that signal intensities were increased in lysates from KO mice when we probed with an antibody directed against a glycosylation-specific epitope of α-DG, i.e. IIH6C4 (**Figure 5C**). Additionally, we observed a shift towards higher molecular weights in KO samples.

We next performed immunostainings of skeletal muscle cross sections of 12-month-old mice with antibodies directed against oligomannose (**Figure 5D** and **Supplementary Figure 4A**), Con A (**Figure 5E** and **Supplementary Figure 4B**), PNA (**Figure 5F** and **Supplementary Figure 4C**), and the glycosylation-specific epitope of α-DG (**Figure 5G** and **Supplementary Figure 4D**). In accordance with our immunoblot results Con A signal intensities did not differ between genotypes, while we observed increased staining for oligomannose, PNA, and the glycosylation-specific α-DG epitope in KO animals. Signals were absent after deglycosylation of skeletal muscle sections of WT and KO mice with PNGase F (**Supplementary Figure 4E-H**).

In summary, GDP-mannose levels are increased in skeletal muscle of *Gmppa* KO mice, which results in the hyperglycosylation of skeletal muscle proteins including α-DG.

Increased α-DG turnover and myotube degeneration upon *GMPPA* knockdown in myoblasts

To assess whether the myopathy upon disruption of GMPPA is muscle intrinsic, we performed knockdown experiments in primary murine myoblasts followed by differentiation into myotubes. As in *Gmppa* KO mice the knockdown resulted in the hyperglycosylation of α-DG (**Figure 6A**). Myoblasts further allowed us to assess the turnover of α-DG in the presence or absence of GMPPA. We assessed the abundance of α-DG with antibodies directed against the α-DG core 24 h after blocking of protein translation with cycloheximide (CHX). Ubiquitin levels confirmed that CHX treatment was effective. Following transfection with scrambled siRNAs, the abundance of α-DG decreased by 24% without and by 47% upon CHX treatment and

knockdown of GMPPA (**Figure 6A**). This indicates that α-DG turnover is increased upon disruption of GMPPA.

To rule out that loss of GMPPA affects myogenesis per se, we addressed whether knockdown of GMPPA in myoblasts interferes with myogenic differentiation in vitro. Primary myoblasts were differentiated into early myotubes (marked by the expression of MyHC and myogenin) and then transfected with siRNAs directed to *GMPPA*, *DAG1* or a scrambled control (**Figure 6B**). No differences in the fusion index of myoblasts as a marker for myogenic differentiation were observed between the different conditions.

To rule out that early myogenesis is affected by knockdown of GMPPA (20), we also transfected C2C12 myoblasts with siRNA directed to *GMPPA*, *DAG1* or a scrambled control at induction of differentiation (**Figure 6C**). Again, no differences in the fusion index or myotube diameter (Mean±SEM: siDAG1 13.76±0.45 µm, siScr 12.22±0.48 µm, siGMPPA 11.19±0.27 µm; $p>0.05$) were observed when GMPPA was knocked down.

Since *Gmppa* KO mice develop a progressive myopathy, we asked whether myotubes are affected by *GMPPA* knockdown. C2C12 cells were differentiated into late myotubes and then transfected with siRNA against *GMPPA*, *DAG1* or a scrambled control (**Figure 6D**). Knockdown of *GMPPA* caused a decrease in myotube diameter compared to the control suggesting that loss of GMPPA results in the atrophy of myotubes/myofibers. As expected, we also observed a decrease in myotube diameter after knockdown of DAG1.

Taken together, knockdown of *GMPPA* in myoblasts increases its turnover and affects the size of late myotubes.

Hyperglycosylation and decreased abundance of α-DG in AAMR patients

We next addressed whether our in vitro findings also apply in vivo. Indeed, the signals with the antibody directed against the α-DG core epitope were reduced in skeletal muscle sections of *Gmppa* KO mice, while β-DG abundance was unchanged (**Figure 7A,B** and overviews shown in **Supplementary Figure 5A**). Because signal intensities for the α-DG core were reduced in KO samples after prior deglycosylation, we conclude that the core epitope is not masked by

hyperglycosylation (**Supplementary Figure 5B**). Decreased abundance of the α-DG core was further confirmed by immunoblot analyses of both native (**Figure 7C**) and deglycosylated (**Supplementary Figure 5C**) skeletal muscle protein lysates.

We also had access to muscle biopsies from two adult sisters, who suffer from AAMR syndrome, because they are homozygous for the GMPPA variant p.R373P (21). We found an increased staining for the glycosylation-specific epitopes of α-DG (IIH6C4, VIA4) in patient samples compared to a healthy control (**Figure 7D,E**), while the signal intensities for the α-DG core protein were reduced (**Figure 7F**). In agreement with our findings obtained in *Gmppa* KO mice, β-DG signals did not differ (**Figure 7G**), while the distribution of laminin was less homogenous compared to the control (**Figure 7H**). Immunoblot analysis of skeletal muscle lysates showed a reduction of GMPPA abundance and increased signal intensities for both oligomannose and PNA, while signals for Con A and laminin were unchanged (**Figure 7I**) similar to our findings in *Gmppa* KO mice. Moreover, signal intensities with the antibodies IIH6C4 and VIA4, which are directed against glycosylation-specific epitopes of α-DG, clearly confirmed α-DG hyperglycosylation in AAMR patients. Signal intensities with the antibody directed against the α-DG core were reduced (**Figure 7I**). As in KO mice, the immunostaining pattern for the Z-disc protein α-actinin was less organized in biopsies from AAMR patients and lacked the regular pattern observed in control samples (**Figure 7J**). In agreement, the ultrastructural analyses showed disarrayed filaments and loss of the continuity of the Z-discs in AAMR patients compared to the control (**Figure 7K**).

In short, the relevance of our findings in *Gmppa* KO mice is confirmed by the analysis of skeletal muscle biopsies from patients suffering of AAMR-syndrome.

Motor impairment of *Gmppa* KO mice can be rescued by dietary mannose-restriction

Of note, serum mannose concentrations were significantly increased in 3-month-old untreated KO mice (**Figure 8A**). Because mannose is easily taken up in the gastrointestinal tract (22), we considered that mannose serum levels may be normalized by dietary mannose restriction. Control and *Gmppa* KO mice were either fed with a nominally mannose-free diet, in which

mannose was replaced by sucrose, or the regular chow starting from postnatal day 14 up to 12 months of age. The mannose serum concentration in WT mice was largely unaffected by the diet, while mannose levels almost normalized in 3-month-old treated KO mice (**Figure 8A**). Contextual learning in the fear-conditioning paradigm (**Figure 8B**) and the abnormal cortical layering (**Figure 8C** and **Supplementary Figure 6A**) was not improved by dietary intervention at 3 months of age. The progressive loss of hippocampal neurons (**Figure 8D** and **Supplementary Figure 6B**) and Purkinje cells (**Figure 8E** and **Supplementary Figure 6C**), however, was largely attenuated by the diet. The deterioration of motor functions was almost completely prevented in *Gmppa* KO mice as assessed by the foot-base-angle (**Figure 8F**), the latency to fall from a wire mesh (**Figure 8G**), and the weights test (**Figure 8H**). The muscle mass was also almost normalized in treated KO mice (**Supplementary Figure 6D**). While centralized nuclei were drastically increased in the untreated KO cohort, it almost normalized by dietary intervention (**Figure 8I** and **Supplementary Figure 6G,H**). The altered distribution of laminin signals and the decreased mean myofiber diameter were rescued as well by dietary intervention (**Figure 8J** and **Supplementary Figure 6G,H**).

Signal intensities of Western blots of skeletal muscle lysates probed with PNA and antibodies directed against paucimannose, oligomannose, the α-DG core and its glycosylation-specific epitope revealed that the mannose-free diet almost normalized the levels and the glycosylation status of these proteins in *Gmppa* KO mice (**Figure 8K**). Increased phosphorylation of ERK 1/2 indicating that MAPK/ERK signaling is activated in KO muscle, largely normalized as well. These results show that neurodegeneration and motor impairment can be largely prevented by post-weaning dietary mannose restriction of *Gmppa* KO mice but does not improve defects of brain development.

Discussion

Up to now, the function of GMPPA and thus the pathophysiology of the AAMR-syndrome remained largely unclear, because GMPPA itself lacks enzymatic activity (6). This is explained by a 2 aa insertion in a highly conserved motif near the catalytic pocket of GMPPA's N-terminal nucleotidyl-transferase domain (aa 3-194) (16, 23), which is shared with other enzymes that transfer nucleotides onto phosphosugars (24). The absence of GDP-mannose-pyrophosphorylase activity for GMPPA is also confirmed by our data. Because GMPPA can still bind GDP-mannose (25) and the presence of GMPPA inhibited the activity of GMPPB in a GDP-mannose dependent manner, our findings further suggest that GMPPA acts as an allosteric feedback inhibitor of GMPPB. In agreement with this function, GMPPA and GMPPB directly interact with each other. Notably, this interaction requires the intact C-terminal part that includes a hexapep domain (aa 286-319), which is likewise found in several members of the transferase families (26). Interestingly, the interaction is abolished in the disease-associated C-terminal GMPPA variant p.T334P, which lacks inhibition of GMPPB activity.

As an allosteric feedback inhibitor of GMPPB, loss of GMPPA is predicted to result in increased GDP-mannose levels, which was indeed observed in skeletal muscles of *Gmppa* KO mice. Because the increase in GDP-mannose levels can cause imbalances in glycosylation reactions by inhibiting enzymes with the use of other NDP-sugars or by favoring reactions displaying a high KM for this NDP-sugar, we performed a glycome analysis by mass spectrometry and found a significant increase in high-mannose *N*- and *O*-glycan structures. Also, the signals for the carbohydrate-binding lectin PNA as well as for antibodies directed against oligo- and paucimannose were increased in skeletal muscle protein lysates or tissue sections of *Gmppa* KO mice. More specifically, we identified α-DG as a hyperglycosylated protein in skeletal muscles of *Gmppa* KO mice, which we also confirmed in skeletal muscle biopsies from AAMR patients.

Typically dystroglycanopathies either result from primary dystroglycan defects or from α-DG hypoglycosylation, which weakens it's binding to the ECM and thus causes membrane fragility (27). The binding depends on the repeating disaccharide [-3-xylose-alpha1,3-glucuronic acid-beta1-], which is attached by like-acetylglucosaminyl transferase (LARGE) (28, 29). Notably, LARGE is mutated in some forms of muscular dystrophies (30). Its transgenic overexpression resulted in α-DG hyperglycosylation and thereby increased laminin binding (31). Therefore, it was proposed that LARGE overexpression might be a therapeutic strategy for dystroglycanopathies (31). However, LARGE overexpression decreased maximal muscle force (31) and worsened the muscle pathology in fukutin-related protein (FKRP) knock-down mice (32). In light of these findings, this strategy might be dangerous because the hyperglycosylation of α-DG may compromise the maintenance of skeletal muscle fibers.

We considered that the turnover of hyperglycosylated α-DG may be increased and may thus lead to less abundance of the α-DG core protein. Indeed, less abundance of the α-DG core protein was suggested by our analyses of skeletal muscles of KO mice and skeletal muscle biopsies from AAMR-patients. This suggests that there is even more glycosylation per core protein as suggested by our western blots. Excluding the possibility that the hyperglycosylation may mask the α-DG core epitope, the α-DG core abundance was decreased in KO mice after enzymatic deglycosylation of skeletal muscle samples. Moreover, siRNA mediated knockdown of GMPPA in myoblasts caused α-DG hyperglycosylation and increased its turnover as judged by immunoblot analysis after blocking protein translation. The reduced size of myotubes upon knockdown of GMPPA is in agreement with muscle intrinsic effect of GMPPA loss-of-function. The decreased abundance and the hyperglycosylation of α-DG may explain the irregular distribution of its ECM binding partners such as laminin.

The balanced supply of GDP-mannose as a sugar donor for both *N*- and *O*-glycosylation (6) requires the interplay between GMPPA and GMPPB, which catalyzes the production of GDP-mannose from mannose-1-phosphate and GTP. Mutations in phosphomannomutase 2 (PMM2) (33), which converts mannose-6-phosphate to mannose-1-phosphate, and mutations

in phosphomannose isomerase (PMI) (34), which facilitates the interconversion of fructose 6-phosphate and mannose-6-phosphate, decrease the availability of GDP-mannose and thus result in the hypoglycosylation of glycoproteins. Mannose is easily taken up in the gastrointestinal tract (35) and together with glucose-derived mannose as well as mannose released from glycans undergoing degradation (36) contributes to the mannose pool used for glycoconjugate synthesis (35). Thus, external mannose supplementation rescued the complex symptoms of patients (34) with PMI defects and was successful in treating PMM2 hypomorphic mice (37). In *Gmppa* KO mice, however, we found serum mannose concentrations to be strongly increased, which may reflect increased release from glycans and/or increased generation of mannose from glucose. Although only ~2% of mannose entering the cell is used for glycosylation (35), the higher systemic mannose levels may contribute to the larger pool of GDP-mannose in *Gmppa* KO mice and thus hyperglycosylation. Therefore, we assessed whether increased systemic mannose concentration and the hyperglycosylation in *Gmppa* KO mice can be mitigated by dietary mannose restriction and fed both control and KO mice on a diet, in which mannose was replaced by sucrose starting at postnatal day 14. This almost normalized the mannose concentration in the serum of 3-month-old KO mice. Moreover, α-DG hyperglycosylation and the decrease in the abundance of the α-DG core largely normalized. Importantly, the deterioration of the motor performance and neuron loss were also largely prevented by dietary intervention. Since cortical development is already largely established at postnatal day 14 in mice (38), when we started with dietary mannose restriction, it came as no surprise that cortical layering and cognitive functions as assessed by fear conditioning were not improved. Therefore, it will be important to address whether dietary intervention in pregnant mice can be beneficial for cortex development and cognitive functions of KO offspring in future studies.

Taken together, we here establish a role of GMPPA as an allosteric feedback inhibitor of GMPPB. This results in increased GDP-mannose tissue levels in GMPPA deficiency and increases the incorporation of mannose into glycoproteins including α-DG. Because the

hyperglycosylation increases the turnover of α-DG, it lowers its overall abundance, which likely contributes to the GMPPA-associated myopathy. Dietary mannose restriction is successful to correct α-DG glycosylation and abundance and largely prevents neuron loss and deterioration of motor functions in *Gmppa* KO mice.

Materials and Methods

To study the function of GMPPA and the consequences of its disruption we investigated *Gmppa* KO mice and cell culture models. Experiments were performed in a C57BL/6 background in the 4th generation. Mice were housed in a 12 h light/dark cycle and had access to mouse chow *ad libitum* (9% fat, 24% protein, 67% carbohydrates including 1% of free mannose). Treatment cohorts were fed with nominally mannose-free food, in which free mannose had been replaced by saccharose. Littermates of the same sex were randomly assigned to experimental groups. End points were termination of treatment and moribundity for mice in accordance with Institutional Animal Care and Use Committee guidelines. Experiments were conducted blind as to cell and mouse and human genotypes. Figure legends include details of replicate experiments used to generate data sets. All animal experiments were approved by the „Thüringer Landesamt für Lebensmittelsicherheit und Verbraucherschutz (TLLV)“. In behavioral experiments for the initial characterization groups comprised 6 female and 6 male mice per genotype. For the intervention study the groups consisted of 6 females and 5 males per condition and genotype. For tissue extraction and histology male mice were used.

Targeted inactivation of the murine *GMPPA* gene

To disrupt *Gmppa* in mice, we obtained the EUCOMM EPD0621_7_G03 embryonic stem cell clone, which harbors a gene-trap cassette following exon 4 and 6 of the *Gmppa* gene. This clone was injected into C57BL/6 donor blastocysts and transferred into foster mice. The resulting chimeric mice were subsequently mated with FLPe delete (12) and Cre deleter (13) mice in order to generate homozygous KO mice devoid of exon 5. ES cell clones and tail biopsies from chimeric mice were analyzed by Southern Blot using EcoRI and a probe of 453 bp binding to Intron 2 of the *Gmppa* locus.

Motor performance and fear conditioning

Beam-walk test: Mice were trained to walk on a horizontal beam. The foot base angle was measured at toe-off positions of the hind-paws using single video frames from recordings of beam walking mice with ImageJ (free software available at www.fiji.sc) (14). For statistical analyses, the mean of two independent trials was taken.

Kondziela´s inverted screen test: The mouse was placed in the center of a wire mesh, the screen was inverted and the time was taken until the mouse fell off the screen. If the mouse did not fall off the screen, the experiment was terminated after 70 s (39).

Weights test: A mouse was held on its tail base and allowed to grip weights (2.8; 9.2; 15.4; 19; 34.2; 42.5; 50; 60.4; 73; 86.5 and 103.0 g) with the fore-paws. If the mouse was able to hold the weight for ≥ 3 sec, the procedure was repeated with the next heavier weight. If the mouse failed to hold the weight for 3 sec, the procedure was repeated for the same weight. If the mouse failed at 3 consecutive events, the experiment was terminated.

Fear conditioning: Mice were placed in a chamber (d 17 x w 17 x h 25 cm, Plexiglas wall, 4 lux light, 70 % ethanol, fan speed 100 %) and allowed to explore the surrounding area for 180 s. A tone was played for the following 20 s (9 kHz, volume 20 %, 80 dB) paired with a foot shock (US, 0.7 mA for 2 s) applied in the last 2 s via the metal grid. After additional 60 s mice were returned to their home cages. After 24 h, the cued test was performed to assess the tone-shock association. Therefore, mice were placed in a differently shaped box with altered color pattern (caro patterned wall, white floor), lightening (2 lux), odor (3 % acetic acid) and fan speed (50 %). Mice were allowed to explore the new area for 180 s before the tone was applied for 180 s. After additional 60 s mice were transferred back into their home cages and allowed to relax for 2 h. After 2 h they were placed in the same context as during acquisition (Plexiglas walls, metal grid floor, lightening 4 lux, odor 70 % ethanol, fan speed 100 %), and observed for 180 s. Animals were video recorded the whole time for automatic detection of freezing by ANY-maze software (Stoelting). For freezing detection, videos were manually analyzed. Freezing time was presented as percentage of the investigated 60 s intervals.

Electrophysiological analysis of peripheral nerves

Anesthetised mice (100 mg/kg ketamine & 16 mg/kg xylazine) were placed on a heating pad. One needle electrode (WE30030.1H10, Science Products) was inserted near the base of the tail and a second one 30 mm distal to the stimulation site close to the tip of the tail. For the analysis of motor fibres, the stimulus was applied via the proximal electrode and the response recorded with the distal electrode. For the analysis of sensory fibres, the stimulus was applied via the distal electrode and recorded from the proximal electrode. The amplitude of the rectangular stimulation pulses (duration 0.1 ms) was increased stepwise from 1 V to 15 V. Sum action potentials wee filtered (highpass 20 Hz, low-pass 10 kHz), digitized (sampling 20 kHz) and averaged.

Real-time quantitative PCR

RNA was isolated by trizol-chloroform extraction. RNA was reverse-transcribed using the SuperScriptIII Transcriptase kit (Invitrogen). For quantitative PCR (qPCR) the innuMix qPCR MasterMix (Analytik Jena) and Taqman Gene Expression Assays (Thermo Fisher Scientific) for *Gapdh* (4331182, Assay-identifier: Mm99999915_g), and *Gmppa* (4331182, Assay-identifier: Mm00505084_m1) were used with 100 ng cDNA.

Protein isolation of cells and tissue lysates

Cells were harvested and lysed in RIPA buffer (50 mM Tris-HCl pH 7.4, 150 mM NaCl, 1% (v/v) NP-40, 1% (w/v) sodium deoxycholate, 0.1% (w/v) SDS, 1mM EDTA, and complete protease inhibitor (Roche).

Tissue lysates were prepared with the Ultra-Turrax T8 tissue homogenizer (IKA-WERKE) in RIPA buffer. After sonication, homogenates were spun down at 16,900 g to remove nuclei and insoluble debris. The supernatant was stored at -80°C until further use.

Western Blot

Proteins were denatured at 90°C for 5 min in Laemmli buffer. After separation by SDS-PAGE proteins were transferred onto PVDF membranes (Whatman). Membranes were blocked in 1% BSA and incubated with primary antibodies at appropriate dilutions overnight at 4°C. The following primary antibodies were used: rabbit anti-GMPPA (Proteintech) 1:500, rb anti-GMPPB (Abcam, ab125421) 1:500, rabbit anti-GAPDH (Santa Cruz, sc-25778) 1:1,000, rabbit anti-Myc (Millipore, 06-549) 1:1,000, rabbit anti-FLAG M2 (Sigma-Aldrich, F7425) 1:1,000, mouse anti-MBP (Sigma-Aldrich, M6295) 1:4,000, mouse anti-GST (gift of Jürgen Wienands, Institute of Cellular and Molecular Immunology at the University Medical Center Göttingen, Germany), rabbit anti-laminin (Abcam, ab11575) 1:500, rabbit anti-nidogen (Abcam, ab14511) 1:500, rabbit anti-collagen IV (Abcam, ab6586) 1:500, self-made antibodies mouse anti-oligomannose and mouse anti-paucimannose 1:50 (gift from Rüdiger Horstkorte, Institute for Physiological Chemistry, Martin-Luther-University Halle-Wittenberg, Halle, Germany), mouse anti-α-DG IIH6C4 (Millipore, 05-593) 1:250, mouse anti-α-DG VIA4 (Millipore, 05-298) 1:250, sheep anti-core-α-DG (R&D Systems) 1:1,000, mouse anti-ubiquitin (Thermo Fischer, 13-1600) 1:1,000, 1:500, rabbit anti-P-ERK 1/2 (Cell Signaling, 4370) 1:4,000, rabbit anti-ERK 1/2 (Cell Signaling, 4695) 1:4,000. Primary antibodies were detected with horseradish peroxidase-conjugated secondary antibodies. To detect glycans we used the following lectins: biotin-PNA (Vector labs) and biotin-Con A (gift from Dr. Christian Thiel, Group Congenital Disorders of Glycosylation, University Hospital Heidelberg, Germany), which were detected with horseradish peroxidase-conjugated streptavidin. Detection was performed with the SuperSignal Western Blot Enhancer Kit (Thermo Fisher Scientific). The quantification of bands was done with ImageJ. All blots were repeated at least once.

Co-immunoprecipitation and GST-pulldown

HEK-293T cells (from ATCC, Germany) were either transfected with human cDNAs encoding GMPPA-Myc, GMPPB-FLAG, GMPPA-T334P-Myc, GMPPA-N182D-Myc, FLAG-GMPPA, GMPPB-FLAG plasmids and/ or Myc-tagged cDNA constructs missing either the C- (GMPPA

aa1-205) or N-terminal part (GMPPA aa206-420) using the Lipofectamine 2000 reagent (Invitrogen). After 24 h cells were lysed (20 mM imidazole pH 8.0, 150 mM NaCl, 2mM $MgCl_2$, 300 mM sucrose, 0.25% (v/v) TritonX-100) and centrifuged at 16,900 g. The supernatant was incubated with either Myc- or FLAG-coupled agarose beads overnight at 4°C. The beads were washed and boiled at 90°C for 10 min in Laemmli sample buffer.

Recombinant human GST-GMPPB and MBP-GMPPA proteins were generated in E. coli (from ATCC, Germany) using the pGEX4T1 and pMal-c2X or pMAL-c5X plasmids and purified on glutathione-agarose (Sigma-Aldrich) or amylose-resin (New England Biolabs). Comparable amounts of protein were pre-incubated in lysis buffer (20 mM imidazole pH 8.0, 150 mM NaCl, 2mM $MgCl_2$, 300 mM sucrose, 0.25% (v/v) TritonX-100) and centrifuged at 16,900 g. The supernatant was incubated with GSH-agarose beads for 45 min at 4°C, washed and protein complexes were eluted with Laemmli buffer by boiling at 90°C for 5 min. After separation of proteins by SDS-PAGE, Western blot analyses were performed with anti-MBP and anti-GST antibodies.

Histology and immunohistochemistry

Muscle tissue was cryo-sectioned into 5 µm thick sections. For histological analyses sections were stained with hematoxylin/eosin (Sigma-Aldrich). Images were captured with a Zeiss AxioLab A1 microscope and further analyzed by ImageJ.

For the NADH diaphorase staining cryo-sections were incubated for 30 min at 37°C in NADH solution (8mg NADH/5 ml 0.05M Tris buffer, pH 7.6) and Nitro-Blue Tetrazolium (NBT) solution (10mg NBT/5 ml 0.05M Tris buffer, pH 7.6) at a 1:1 ratio. Afterwards, sections were washed and excessive NBT was removed with acetone. Images were captured with a Zeiss AxioLab A1 microscope and further analyzed by *ImageJ*.

For Picro-Sirius red staining analyses, sections were stained with hematoxylin (Sigma-Aldrich). After washing sections were stained in 0.5% (w/v) Picro-Sirius red solution (Sigma Aldrich) for 1 h and then washed in acidified water. Images were captured with a petrographic microscope (AxioImager Z.2, Zeiss) and further analyzed by ImageJ.

For TUNEL stainings, cryosections were processed according to the manufacturer´s instructions (11684795910 Roche).

Brain tissue was cryo-sectioned into 12 µm thick sections. Immunfluorescence stainings were performed in Shandon chambers (Thermo Scientific). Sections were fixed with 4% PFA and rinsed in PBS. 0.25% (v/v) Triton-X in 1xPBS was used to permeabilize cells. After blocking, following primary antibodies were applied overnight at 4°C: rabbit anti-laminin (Abcam, ab11575) 1:200, rabbit anti-nidogen (Abcam, ab14511) 1:200, rabbit anti-collagen IV (Abcam, ab6586) 1:100, mouse anti-oligomannose and anti-paucimannose (Rüdiger Horstkorte) both 1:50, mouse anti-α-DG IIH6C4 (Millipore, 05-593) 1:100, mouse anti-α-DG VIA4 (Millipore, 05-298) 1:100, goat anti-α-DG (Abcam, ab136665) 1:100, rabbit anti-β-DG (GeneTex, GTX124225) 1:100, mouse anti-α-actinin (EA-53, Abcam, ab9465) 1:200, mouse anti-myosin heavy chain IIB (BF-F3, DSHB) undiluted, mouse anti-myosin heavy chain IIA (sc-71, DSHB) undiluted, mouse anti-myosin heavy chain 7 (A4.840, DSHB) undiluted, mouse anti-NeuN (Millipore, MAB377) 1:250, rabbit anti-calbindin (D28-K, Swant, CB38) 1:250. To detect glycans we used biotin PNA (Vector labs) and biotin Con A (gift from Dr. Christian Thiel) in a dilution of 1:50. Corresponding secondary antibodies were obtained from Invitrogen. Nuclei were stained with DAPI 1:10,000 (Invitrogen). Sections were mounted with Fluoromount-G (Southern Biotech). Images were taken with a Zeiss LSM880 Airyscan confocal microscope. Z-projections with average intensities processed with ImageJ are shown. The acquisition parameters and image processing were identical.

Deglycosylation

For the analysis of deglycosylated proteins by Western blot proteins an enzymatic Carborelease kit (QA Bio) containing PNGase F (Chryseobacterium meningosepticum), *O*-glycosidase (Streptococcus pneumoniae), neuraminidase (Arthrobacter ureafaciens), β-galactosidase (Streptococcus pneumoniae), β-N-acetylglucosaminidase (Streptococcus pneumonia) as well as α-mannosidase (Jack Bean, QA Bio) were used following the

manufacturer's instructions for denaturing conditions. Afterwards, immunoblotting was performed as described above.

For immunostainings of deglycosylated sections, cryo-tissue sections were incubated with 0.3% (w/v) SDS and 60 mM DTT for 10 min at 65 °C, followed by washing with PBS and treatment with 10 U/µl PNGase F (Promega) in 50 mM Na_2HPO_4 supplemented with 1% (v/v) NP-40 at 37 °C for 1.5 h. Afterwards, immunofluorescence staining was performed as already described.

Proximity ligation assay

Proximity ligation assays (PLA) were performed with the Duolink in situ red starter kit mouse/rabbit (DUO92101) according to the manufacturer´s instructions (Sigma-Aldrich) with rabbit anti-GMPPA (Proteintech) and mouse anti-GMPPB (Novus Biologicals) antibodies in a 1:25 dilution.

Enzyme activity assays

Recombinant human GST-GMPPA, MBP-GMPPA, GST-GMPPB, MBP-GMPPB and variant proteins were generated in E. coli using the pGEX4T1 and pMal-c2X or pMAL-c5X plasmids and purified on glutathione-agarose (Sigma-Aldrich) or amylose-resin (New England Biolabs). GDP-mannose-pyrophosphorylase activity of recombinant enzymes was measured by determining the quantity of inorganic phosphate generated from pyrophosphate in the presence of mannose-1-phosphate (150 µM), GTP (300 µM) and excess pyrophosphatase (1 U/ml; Merck) in assay buffer (25 mM Tris-HCl (pH 7.5), 150 mM NaCl, 4 mM $MgCl_2$, 0.01% (v/v) Tween 20, 1 mM dithiothreitol in ultrapure water supplemented with protein inhibitor cocktail (Roche)) at 37°C for 40 min as described previously (17). Biochemical reactions were terminated by adding equal volumes of revelation buffer (0.03% (w/v) malachite green (Sigma), 0.2% (w/v) ammonium molybdate, 0.05% (v/v) Triton X-100 in 0.7 M HCl) at 30°C for 5 min and absorbance measured at 650 nm. For measuring GMPPB activity in the presence of GMPPA, 20 ng/µl GMPPB was mixed with 20 ng/µl GMPPA in assay buffer supplemented with

pyrophosphatase 1 U/ml, 300 µM GTP, 150 µM mannose-1-phosphate and increasing GDP-mannose concentrations.

Sugar measurements

Blood was taken from unfasted mice and incubated on ice for 15 min. Samples were centrifuged for 10 min at 4°C and 4,000 g. Sugars were measured in the supernatant with the D-mannose, D-fructose, D-glucose kit (Megazyme, K-MANGL).

Mass spectrometry analysis of skeletal muscle proteins

Homogenized quadriceps muscle samples were lysed in RIPA buffer followed by reduction, alkylation and subsequent acetone precipitation. Protein pellets were digested into peptides, labeled with 10plex Tandem Mass Tags (Thermo Fisher) and fractionated by high pH reverse phase chromatography, as described earlier (40). The resulting fractions were combined into 24 pools and analyzed in an Orbitrap Fusion Lumos Tribrid Mass Spectrometer (Thermo Fisher) using a synchronous precursor selection (SPS)/MS3 method (41). Raw data were processed using Proteome Discoverer v2.0 (Thermo Fisher) and searched against a Uniprot mouse database using Mascot v2.5.1 (Matrix Science). Differential expression analysis was performed using limma (42). The mass spectrometry proteomics data were deposited to the ProteomeXchange Consortium via the PRIDE (43) partner repository with the dataset identifier PXD014260 (Reviewer account details: Username: reviewer61426@ebi.ac.uk<mailto:reviewer61426@ebi.ac.uk>; Password: MizeK1Tm). Gene set enrichment analysis (GSEA) was performed using WebGestalt (44).

Glycome analysis of skeletal muscle

Mice were fasted for 24 h. Protein lysis was performed in lysis buffer (50 mM Tris-HCl, 100 mM NaCl, 1mM EDTA and proteinase inhibitor cocktail). Samples were sonicated and then centrifuged at 4,000 g at 4°C and the supernatant recovered. For *N*-glycan and *O*-glycan analysis, 200 µg proteins were dissolved in PB pH 6.5 (250 mM NaH_2PO_4, 250 mM Na_2HPO_4)

and SDS was added to a final concentration of 1% (w/v). Proteins were denatured at 95°C for 5 min. The buffer was diluted to 160 mM with water and Ipegal at a final concentration of 1% (w/v). Next, *N*-glycan release was performed using 1 U of PNGase F (N-Zyme Scientifics). *N*-glycans were subsequently cleaned up, permethylated and measured by MALDI-TOF mass spectrometry as described earlier (45). *O*-glycans were released with $NaOH/NaBH_4$ and purified over self-made C18/Dowex H^+ columns followed by a methanolic desalting step in the vacuum centrifuge and a permethylation reaction. The spectra were acquired in *m/z* 300–2000 region in the positive ion mode $[M+Na]^+$. For every spectrum acquisition, 10,000 shots were collected. The spectra were acquired at 100 Hz frequency. Detector gain was set up to 1638V and the analog offset was 51 mV.

Experiments using primary myoblasts

Primary myoblasts isolated from WT mice or C2C12 cells (from ATCC, Germany) were seeded in growth medium (F10 (Gibco), 20% (v/v) FBS (Gibco), 2% pentamycin/streptomycin (Gibco), 2.5 ng/ml bFGF (Gibco)) on collagen coated culture dishes. The next day, cells were treated with differentiation medium (DMEM (Sigma-Aldrich), 5% (v/v) HS (Gibco), 2% pentamycin/streptomycin in (Gibco)) and allowed to differentiate for 2 days. Then cells were transfected with siRNAs against either control (siScr), dystroglycan (siDAG1, Dharmacon) or GMPPA (siGMPPA, Novus Biologicals) according to the manufacturer's protocol using Lipofectamine RNAiMax (Invitrogen). After four days of differentiation, cells were fixed with 2% PFA, permeabilized, blocked, and stained with antibodies directed against myogenin (F5D, DSHB) 1:2 and myosin heavy chain (MF20, DSHB) 1:2 overnight at 4°C followed by an incubation with the corresponding secondary antibodies (Invitrogen). Nuclei were stained with DAPI (10 µg/ml, Invitrogen). Images were taken with the Axio Imager and Axio Observer.Z1 (Carl Zeiss) and further analyzed with the Zen software (Carl Zeiss).

For cycloheximide (CHX) experiments, primary myoblasts were seeded, differentiated, and transfected as described above. After 3 days, cells were treated with 8 µg/ml cycloheximide for 24 hours. Then cells were harvested with RIPA buffer. After sonication homogenates were

spun down at 16,900 g to remove nuclei and insoluble debris. The supernatant was stored at -80°C.

Experiments using C2C12 myoblasts

C2C12 cells were seeded in growth medium (DMEM (Sigma-Aldrich), 10% (v/v) FBS (Gibco), 2% (v/v) pentamycin/streptomycin (Gibco). The next day, cells were treated with differentiation medium (DMEM (Sigma-Aldrich), 2% HS (Gibco)) and allowed to differentiate. Transfection with siRNAs against either control (siScr), dystroglycan (siDag1) or GMPPA (siGMPPA) was carried out according to the manufacturer's protocol using Lipofectamine RNAiMax (Invitrogen). Fixation and immunostaining were performed as described above.

GDP-mannose measurements

Mice were sacrificed, organs dissected and immediately frozen in liquid nitrogen. Organ homogenates were run on high-performance liquid chromatography with a modified gradient to enhance separation of NDP-sugars as described previously (7).

Electron microscopy

The human biopsies were immersed in 2.5% (v/v) glutaraldehyde (EMS Cat 16210) followed by two washes in cacodylate buffer (EMS Cat 21300) at pH 7.2 and 0.15 M and post-fixation done in 1% (v/v) osmium tetraoxide (EMS Cat 19100), followed by two washes in cacodylate buffer and tissue dehydrated in the following progressive ethyl alcohol concentrations at 30%, 50%, 70%, 80%, 96% and 100% (v/v). For an adequate infiltration, muscle samples were changed to propylene oxide (EMS Cat 20401). The infiltration was carried out with epoxy resin. The procedure described was carried out in a Leica EM TP automatic processor. Processed biopsies were cut in 75 nm thick sections and mounted on 200 mesh copper grids. The contrast was attained with 5% (w/v) uranyl acetate (EM Grade) and lead citrate with Reynold's method, and the samples analyzed in a Transmission Electron Microscope FEI model Tecnai BioTwin at 80 kV.

Mice were perfused transcardially with 4% PFA and 2.5% glutaraldehyde in PBS. Sciatic nerve was removed and post-fixed. Afterwards, nerves were washed with 0.1 M cacodylate buffer pH 7.3 and post-fixed in 0.1 M cacodylate buffer. Tissue was dehydrated in the following progressive acetone concentrations at 30%, 50%, 70%, 90% and 95% and 100% (v/v). For contrast, 1% (w/v) uranyl acetate was added to 50% (v/v) acetone. The infiltration was carried out with epoxy resin. Processed biopsies were cut in 50 nm thick sections (Reichert Ultracut S, Leica) and analyzed in a Transmission Electron Microscope JEM 1400 (JEOL) at 80 kV.

Statistical analysis

For statistical analysis, raw data were analyzed for normal distribution with the Kolmogorov-Smirnov test or with graphical analysis using the Box-Plot and QQ-Plot. If appropriate we either used 1-way ANOVA, 2-way ANOVA or Student's t-test. * indicates $p<0.05$, ** $p<0.005$ and *** $p<0.0005$. For all data, means with standard error of the mean (SEM) are shown.

Study approval

All animal experiments were approved by the „Thüringer Landesamt für Lebensmittelsicherheit und Verbraucherschutz (TLLV)". For tests with samples of AAMR syndrome patients, who underwent muscle biopsy as part of the diagnostic work up because of progressive muscle weakness, informed consent was obtained that part of the specimen could be used for research purposes. Control samples were obtained from the Telethon Biobank.

Data and Software Availability

Mass spectrometry datasets and MALDI-TOF spectra of glycans are included in the Supplement.

Author Contributions

PF, HH, MJJ, SCS, SM, KB, LL, IK, TK, JM, BM, TH, AKH, JCH, SG, JvM, LG performed experiments and analyzed data. PF, CK, AO, OH, VB, JvM and CAH wrote the paper. PF, RH,

JW, TM, CK, OMM, AO, OH, VB, JvM and CAH interpreted data and contributed to the conceptual design of the study. CAH initiated and coordinated the study.

Acknowledgments

This study was funded by the DFG GRK 2155 ProMoAge to CAH, OH, RH, CK and AO and DFG MA-3975/2-1 to JvM. We thank Emile van Schaftingen and Guido Bommer for continuous support. We thank Katrin Schorr, Manuela Neumann and Johanna Fischer for excellent technical support, Katrin Buder and the Histology and Electron Microscopy Facility of the FLI for EM analysis and Joanna M. Kirkpatrick and the Mass Spectrometry Core Facility of the FLI for support with mass spectrometry. This study is supported by the EUROGLYCAN-*omics* network, E-Rare-3 Joint Transnational Call. The FLI is a member of the Leibniz Association and is financially supported by the Federal Government of Germany and the State of Thuringia.

References

1. Jaeken J. Congenital disorders of glycosylation (CDG): it's (nearly) all in it! *J Inherited Metab Dis.* 2011;34(4):853-8.
2. Belaya K, Rodriguez Cruz PM, Liu WW, Maxwell S, McGowan S, Farrugia ME, et al. Mutations in GMPPB cause congenital myasthenic syndrome and bridge myasthenic disorders with dystroglycanopathies. *Brain.* 2015;138(Pt 9):2493-504.
3. Cabrera-Serrano M, Ghaoui R, Ravenscroft G, Johnsen RD, Davis MR, Corbett A, et al. Expanding the phenotype of GMPPB mutations. *Brain.* 2015;138(Pt 4):836-44.
4. Carss KJ, Stevens E, Foley AR, Cirak S, Riemersma M, Torelli S, et al. Mutations in GDP-mannose pyrophosphorylase B cause congenital and limb-girdle muscular dystrophies associated with hypoglycosylation of alpha-dystroglycan. *Am J Hum Genet.* 2013;93(1):29-41.
5. Jensen BS, Willer T, Saade DN, Cox MO, Mozaffar T, Scavina M, et al. GMPPB-Associated Dystroglycanopathy: Emerging Common Variants with Phenotype Correlation. *Hum Mutat.* 2015;36(12):1159-63.
6. Ning B, and Elbein AD. Cloning, expression and characterization of the pig liver GDP-mannose pyrophosphorylase. Evidence that GDP-mannose and GDP-Glc pyrophosphorylases are different proteins. *Eurpo J Biochem.* 2000;267(23):6866-74.
7. Koehler K, Malik M, Mahmood S, Giesselmann S, Beetz C, Hennings JC, et al. Mutations in GMPPA cause a glycosylation disorder characterized by intellectual disability and autonomic dysfunction. *Am J Hum Genet.* 2013;93(4):727-34.
8. Ervasti JM, and Campbell KP. Membrane organization of the dystrophin-glycoprotein complex. *Cell.* 1991;66(6):1121-31.
9. Ibraghimov-Beskrovnaya O, Ervasti JM, Leveille CJ, Slaughter CA, Sernett SW, and Campbell KP. Primary structure of dystrophin-associated glycoproteins linking dystrophin to the extracellular matrix. *Nature.* 1992;355(6362):696-702.

10. Dumont NA, Wang YX, von Maltzahn J, Pasut A, Bentzinger CF, Brun CE, et al. Dystrophin expression in muscle stem cells regulates their polarity and asymmetric division. *Nat Med.* 2015;21(12):1455-63.
11. Barresi R, and Campbell KP. Dystroglycan: from biosynthesis to pathogenesis of human disease. *J Cell Sci.* 2006;119(Pt 2):199-207.
12. Rodriguez CI, Buchholz F, Galloway J, Sequerra R, Kasper J, Ayala R, et al. High-efficiency deleter mice show that FLPe is an alternative to Cre-loxP. *Nat Genet.* 2000;25(2):139-40.
13. Schwenk F, Baron U, and Rajewsky K. A cre-transgenic mouse strain for the ubiquitous deletion of loxP-flanked gene segments including deletion in germ cells. *Nucleic Acids Res.* 1995;23(24):5080-1.
14. Beetz C, Koch N, Khundadze M, Zimmer G, Nietzsche S, Hertel N, et al. A spastic paraplegia mouse model reveals REEP1-dependent ER shaping. *J Clin Invest.* 2013;123(10):4273-82.
15. Phillips RG, and LeDoux JE. Differential contribution of amygdala and hippocampus to cued and contextual fear conditioning. *Behav Neurosci.* 1992;106(2):274-85.
16. Jin X, Ballicora MA, Preiss J, and Geiger JH. Crystal structure of potato tuber ADP-glucose pyrophosphorylase. *The EMBO journal.* 2005;24(4):694-704.
17. Mao W, Daligaux P, Lazar N, Ha-Duong T, Cave C, van Tilbeurgh H, et al. Biochemical analysis of leishmanial and human GDP-Mannose Pyrophosphorylases and selection of inhibitors as new leads. *Sci Rep.* 2017;7(1):751.
18. Endo T. Aberrant glycosylation of alpha-dystroglycan and congenital muscular dystrophies. *Acta Myol.* 2005;24(2):64-9.
19. Martin PT. Dystroglycan glycosylation and its role in matrix binding in skeletal muscle. *Glycobiology.* 2003;13(8):55R-66R.
20. Cohn RD, Henry MD, Michele DE, Barresi R, Saito F, Moore SA, et al. Disruption of DAG1 in differentiated skeletal muscle reveals a role for dystroglycan in muscle regeneration. *Cell.* 2002;110(5):639-48.

21. Benitez EO, Morales JJ, Munoz LA, Hubner CA, and Mutchinick OM. A Novel GMPPA Mutation in Two Adult Sisters with Achalasia, Alacrima, Short Stature, Dysmorphism, and Intellectual Disability. *Mol Syndromol.* 2018;9(2):110-4.

22. Sharma V, and Freeze HH. Mannose efflux from the cells: a potential source of mannose in blood. *J Biol Chem.* 2011;286(12):10193-200.

23. Sivaraman J, Sauve V, Matte A, and Cygler M. Crystal structure of Escherichia coli glucose-1-phosphate thymidylyltransferase (RffH) complexed with dTTP and Mg2+.*J Biol Chem.* 2002;277(46):44214-9.

24. Jensen SO, and Reeves PR. Domain organisation in phosphomannose isomerases (types I and II). *Biochim Biophys Acta.* 1998;1382(1):5-7.

25. Szumilo T, Drake RR, York JL, and Elbein AD. GDP-mannose pyrophosphorylase. Purification to homogeneity, properties, and utilization to prepare photoaffinity analogs. *J Biol Chem.* 1993;268(24):17943-50.

26. Raetz CR, and Roderick SL. A left-handed parallel beta helix in the structure of UDP-N-acetylglucosamine acyltransferase. *Science.* 1995;270(5238):997-1000.

27. Campbell KP. Three muscular dystrophies: loss of cytoskeleton-extracellular matrix linkage. *Cell.* 1995;80(5):675-9.

28. Inamori K, Yoshida-Moriguchi T, Hara Y, Anderson ME, Yu L, and Campbell KP. Dystroglycan function requires xylosyl- and glucuronyltransferase activities of LARGE. *Science.* 2012;335(6064):93-6.

29. Yoshida-Moriguchi T, Yu L, Stalnaker SH, Davis S, Kunz S, Madson M, et al. O-mannosyl phosphorylation of alpha-dystroglycan is required for laminin binding. *Science.* 2010;327(5961):88-92.

30. Longman C, Brockington M, Torelli S, Jimenez-Mallebrera C, Kennedy C, Khalil N, et al. Mutations in the human LARGE gene cause MDC1D, a novel form of congenital muscular dystrophy with severe mental retardation and abnormal glycosylation of alpha-dystroglycan. *Hum Mol Genet.* 2003;12(21):2853-61.

31. Brockington M, Torelli S, Sharp PS, Liu K, Cirak S, Brown SC, et al. Transgenic overexpression of LARGE induces alpha-dystroglycan hyperglycosylation in skeletal and cardiac muscle. *PLoS One.* 2010;5(12):e14434.

32. Whitmore C, Fernandez-Fuente M, Booler H, Parr C, Kavishwar M, Ashraf A, et al. The transgenic expression of LARGE exacerbates the muscle phenotype of dystroglycanopathy mice. *Hum Mol Genet.* 2014;23(7):1842-55.

33. Matthijs G, Schollen E, Pardon E, Veiga-Da-Cunha M, Jaeken J, Cassiman JJ, et al. Mutations in PMM2, a phosphomannomutase gene on chromosome 16p13, in carbohydrate-deficient glycoprotein type I syndrome (Jaeken syndrome). *Nat Genet.* 1997;16(1):88-92.

34. Niehues R, Hasilik M, Alton G, Korner C, Schiebe-Sukumar M, Koch HG, et al. Carbohydrate-deficient glycoprotein syndrome type Ib. Phosphomannose isomerase deficiency and mannose therapy. *J Clin Invest.* 1998;101(7):1414-20.

35. Sharma V, Ichikawa M, and Freeze HH. Mannose metabolism: more than meets the eye. *Biochem Biophys Res Commun.* 2014;453(2):220-8.

36. Alton G, Hasilik M, Niehues R, Panneerselvam K, Etchison JR, Fana F, et al. Direct utilization of mannose for mammalian glycoprotein biosynthesis. *Glycobiology.* 1998;8(3):285-95.

37. Schneider A, Thiel C, Rindermann J, DeRossi C, Popovici D, Hoffmann GF, et al. Successful prenatal mannose treatment for congenital disorder of glycosylation-Ia in mice. *Nat Med.* 2012;18(1):71-3.

38. Dehay C, and Kennedy H. Cell-cycle control and cortical development. *Nat Rev Neurosci.* 2007;8(6):438-50.

39. Deacon RM. Measuring the strength of mice. *J Vis Exp.* 2013(76).

40. Heinze I, Bens M, Calzia E, Holtze S, Dakhovnik O, Sahm A, et al. Species comparison of liver proteomes reveals links to naked mole-rat longevity and human aging. *BMC Biol.* 2018;16(1):82.

41. Muntel J, Kirkpatrick J, Bruderer R, Huang T, Vitek O, Ori A, et al. Comparison of Protein Quantification in a Complex Background by DIA and TMT Workflows with Fixed Instrument Time. *J Proteome Res.* 2019;18(3):1340-51.

42. Ritchie ME, Phipson B, Wu D, Hu Y, Law CW, Shi W, et al. limma powers differential expression analyses for RNA-sequencing and microarray studies. *Nucleic Acids Res.* 2015;43(7):e47.

43. Perez-Riverol Y, Csordas A, Bai J, Bernal-Llinares M, Hewapathirana S, Kundu DJ, et al. The PRIDE database and related tools and resources in 2019: improving support for quantification data. *Nucleic Acids Res.* 2019;47(D1):D442-D50.

44. Liao Y, Wang J, Jaehnig EJ, Shi Z, and Zhang B. WebGestalt 2019: gene set analysis toolkit with revamped UIs and APIs. *Nucleic Acids Res.* 2019;47(W1):W199-W205.

45. Biskup K, Braicu EI, Sehouli J, Fotopoulou C, Tauber R, Berger M, et al. Serum glycome profiling: a biomarker for diagnosis of ovarian cancer. *J Proteome Res.* 2013;12(9):4056-63.

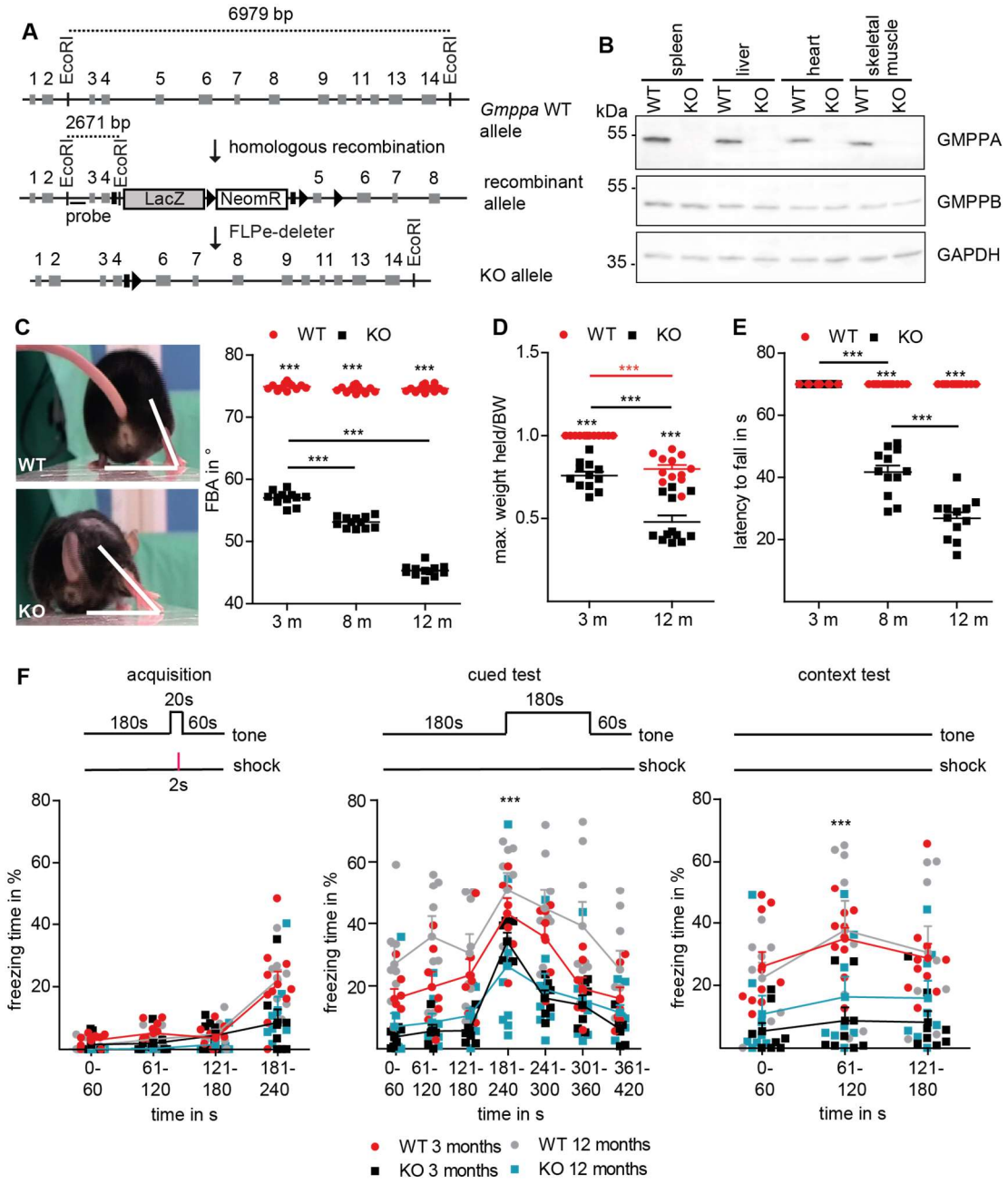

Figure 1. *Gmppa* KO mice show progressive motor deficits and cognitive impairments. A) Genomic structure of the wild-type and targeted *Gmppa* locus. Grey rectangles: exons; black rectangles: Frt sites; black triangles: loxP sites; LacZ: β-galactosidase cassette; NeomR: neomycin-resistance cassette. Black lines: probe-binding sites. **B)** The GMPPA protein is detected in different tissues of WT mice, but is absent in KO samples. GMPPB abundance is not altered in *Gmppa* KO mice. GAPDH served as loading control. **C)** The foot-base-angle (FBA) flattens in KO mice (n=12 mice per group; 2-way ANOVA with Bonferroni post-hoc test). **D)** KO mice can hold less weight with their fore-paws (n=12 mice per group; 2-way ANOVA with Bonferroni post-hoc test). **E)** Aged KO mice fall off earlier from an inverted screen (n=12 mice per group; 2-way ANOVA with Bonferroni post-hoc test). **F)** Cued and contextual fear conditioning test in 3- and 12-month-old WT and KO mice. Freezing behavior during the test was measured as an index of fear memory. For acquisition, mice were placed into a conditioning chamber and were given pairings of a tone and an electric foot-shock. After 24 h mice were either exposed to a different chamber with presentation of the auditory cue (cued test) or the same context as for acquisition (context test). While both genotypes remembered the conditioned stimulus, KO mice were unable to remember the context of the aversive stimulus (n=12 mice per group; 2-way ANOVA with Bonferroni post-hoc test). Quantitative data are presented as mean±SEM with individual data points.

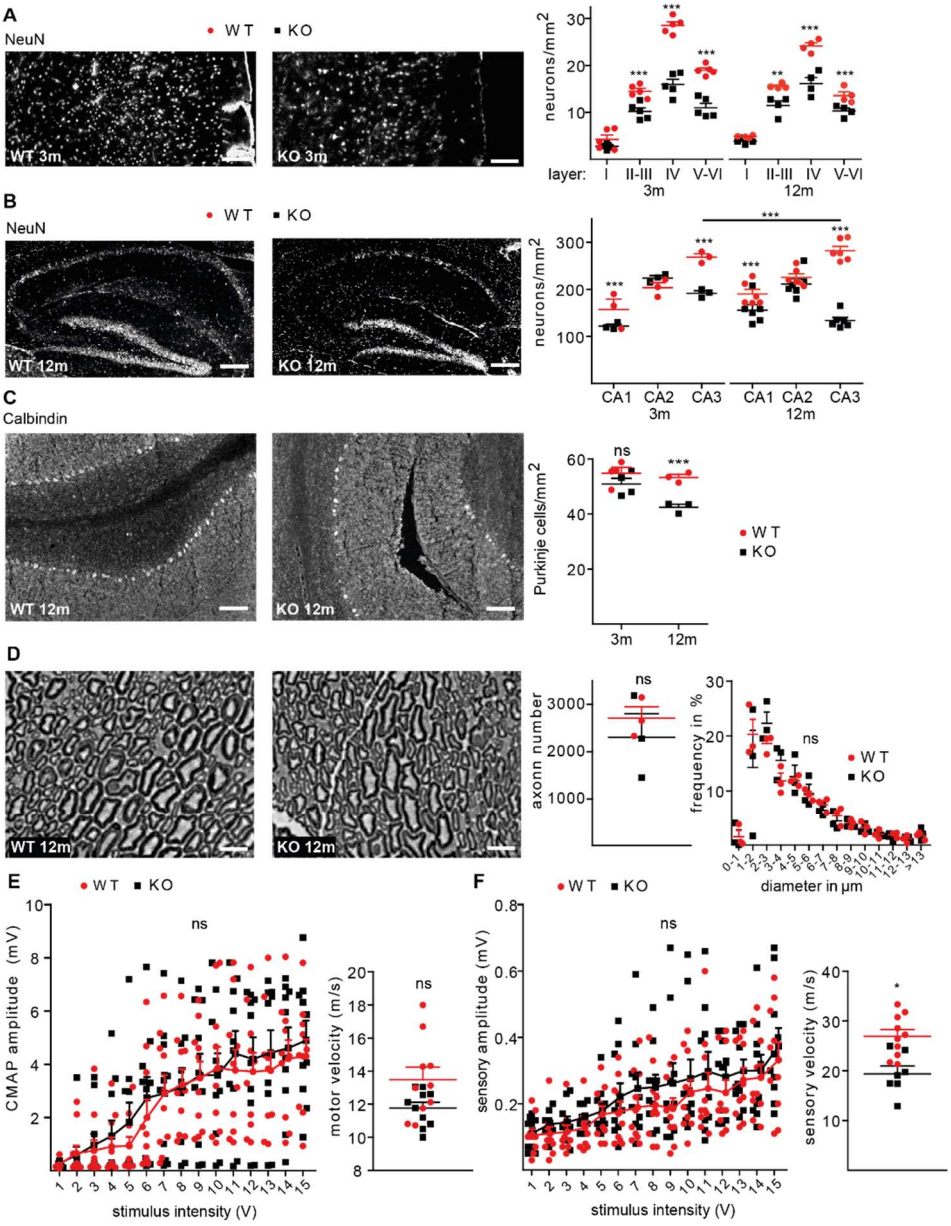

Figure 2. Altered brain development and progressive neuron loss in *Gmppa* KO mice. A) Cortical layering is altered in *Gmppa* KO mice. Sagittal sections of the somatosensory cortex of 3- and 12-month-old WT and KO mice were stained for the neuronal marker NeuN and neurons counted layer-wise (n= 4-6 mice per group; 2-way ANOVA with Bonferroni post-hoc test). Scale bars: 50 µm. **B)** Progressive loss of pyramidal neurons in the hippocampus of *Gmppa* KO mice. Hippocampal sections of 3- and 12-month-old WT and KO mice were stained for NeuN and neurons counted in the CA1, CA2, and CA3 region of the hippocampus (n=3-6 mice per group; 2-way ANOVA with Bonferroni post-hoc test). Scale bars: 125 µm. **C)** Progressive loss of Purkinje cells in *Gmppa* KO mice. Cerebellar sections from 3- and 12-month-old WT and KO mice were stained for calbindin and Purkinje cells counted (n=3-4 mice per group; 2-way ANOVA with Bonferroni post-hoc test). Scale bars: 75 µm. **D)** No obvious morphological changes of sciatic nerves of 12-month-old *Gmppa* KO mice. Toluidine-blue stained semi-thin cross sections of sciatic nerves of 12-month-old WT and KO mice. Total axon numbers and the distribution of axons of different diameters were analyzed (n=3 mice per group; unpaired 2-tailed Student´s t-test for axon number and 1-way ANOVA with Bonferroni post-hoc test for distribution). Scale bars: 5 µm. **E)** Amplitudes of distal compound muscle action potentials (CMAPs) upon stimulation at the tail root and motor nerve conduction velocities are not changed in 12-month-old KO mice (n=10 per group; 1-way ANOVA with Bonferroni post-hoc test). **F)** Sensory amplitudes upon stimulation at the tip of the tail are not changed in 12-month-old KO mice (n=10 per group; 1-way ANOVA with Bonferroni post-hoc test), while sensory nerve conduction velocities are slightly decreased. Quantitative data are presented as mean±SEM with individual data points.

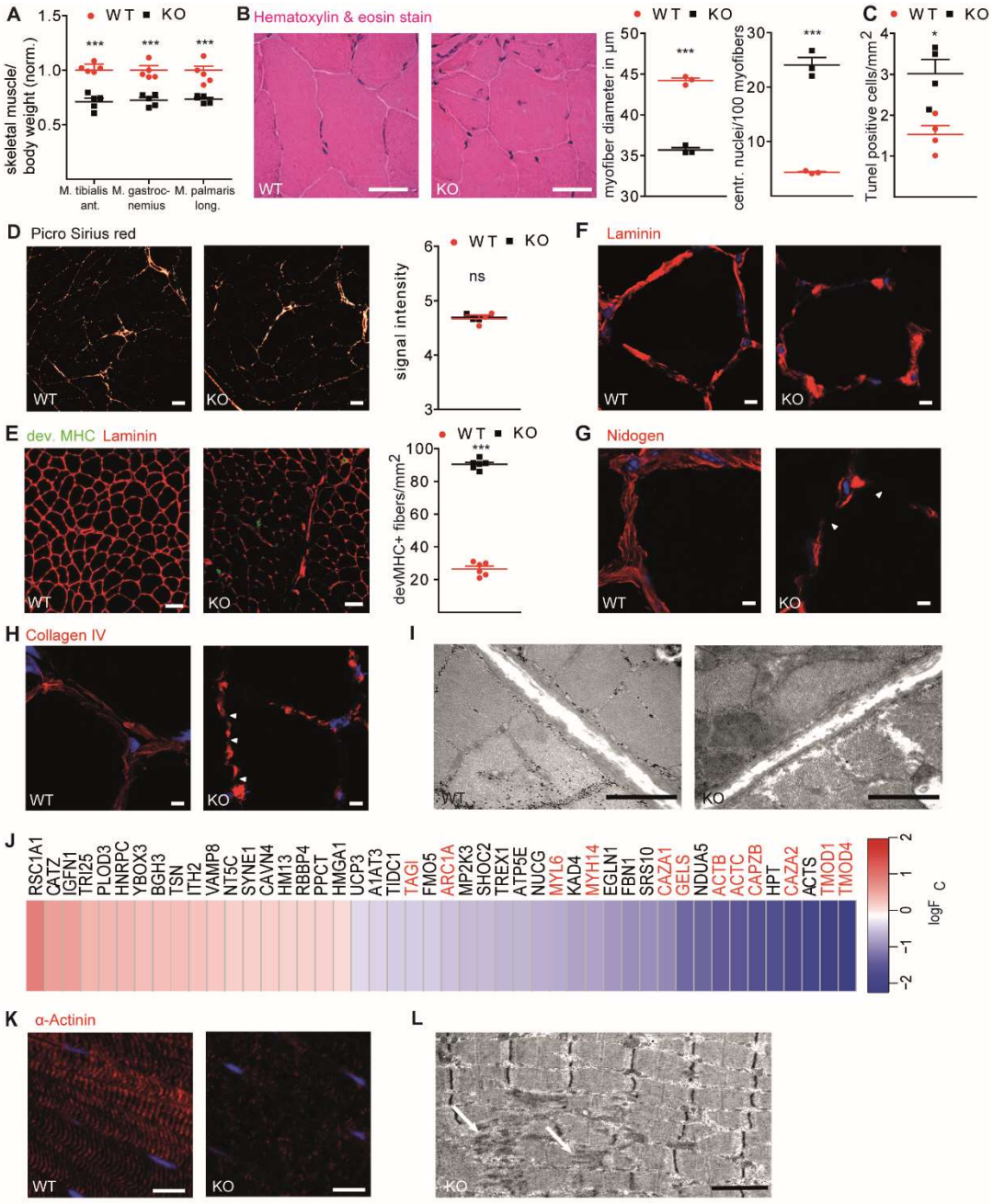

Figure 3. *Gmppa* KO mice develop an age-dependent myopathy. A) Reduced muscle mass in 12-month-old KO mice (n=5 males each; Student's t-test). **B)** Decreased myofiber diameter and centralized nuclei in skeletal muscle sections of 12-month-old KO mice (n=3 mice per group; unpaired 2-tailed Student's t-test). Scale bars: 50µm. **C)** Increased number of Tunel-positive nuclei in KO mice (n=5 mice per group; unpaired 2-tailed Student's t-test). **D)** No relevant skeletal muscle fibrosis at 12 months of age as judged from Picro Sirius red staining (n=3 mice per group; unpaired 2-tailed Student's t-test). Scale bars: 200µm. **E)** Increased number of dev. MHC (green) positive satellite cells in skeletal muscle of 12-month-old KO mice (n=6 mice per group; unpaired 2-tailed Student's t-test). Scale bars: 50µm. **F-H)** Altered distribution of the ECM proteins laminin (F), nidogen (G), and collagen IV (H) in skeletal muscles of 12-month-old KO mice. Overviews and control stainings with secondary antibodies alone are shown in Supplementary Figure 2. Scale bars: 5µm. **I)** Less compact and less tight connection of the endomysial collagen to the myofiber basal lamina in KO samples. Scale bars: 1 µm. **J)** Mass spectrometry analysis of skeletal muscle proteins of 12-month-old WT and KO mice. Proteins significantly up-regulated in KO are shown in red, those down-regulated in blue (threshold q<0.2; n=5 mice per genotype). The red font refers to genes related to muscle contraction. **K)** Irregular α-actinin pattern in skeletal muscle of 12-month-old KO mice (arrowheads). Scale bars: 10µm; n=3 mice per group. **L)** Myofibrillar disintegration with Z band streaming (arrows). Sarcomeres surrounding the lesion show a normal Z band pattern. Scale bar: 2 µm. Quantitative data are presented as mean±SEM with individual data points.

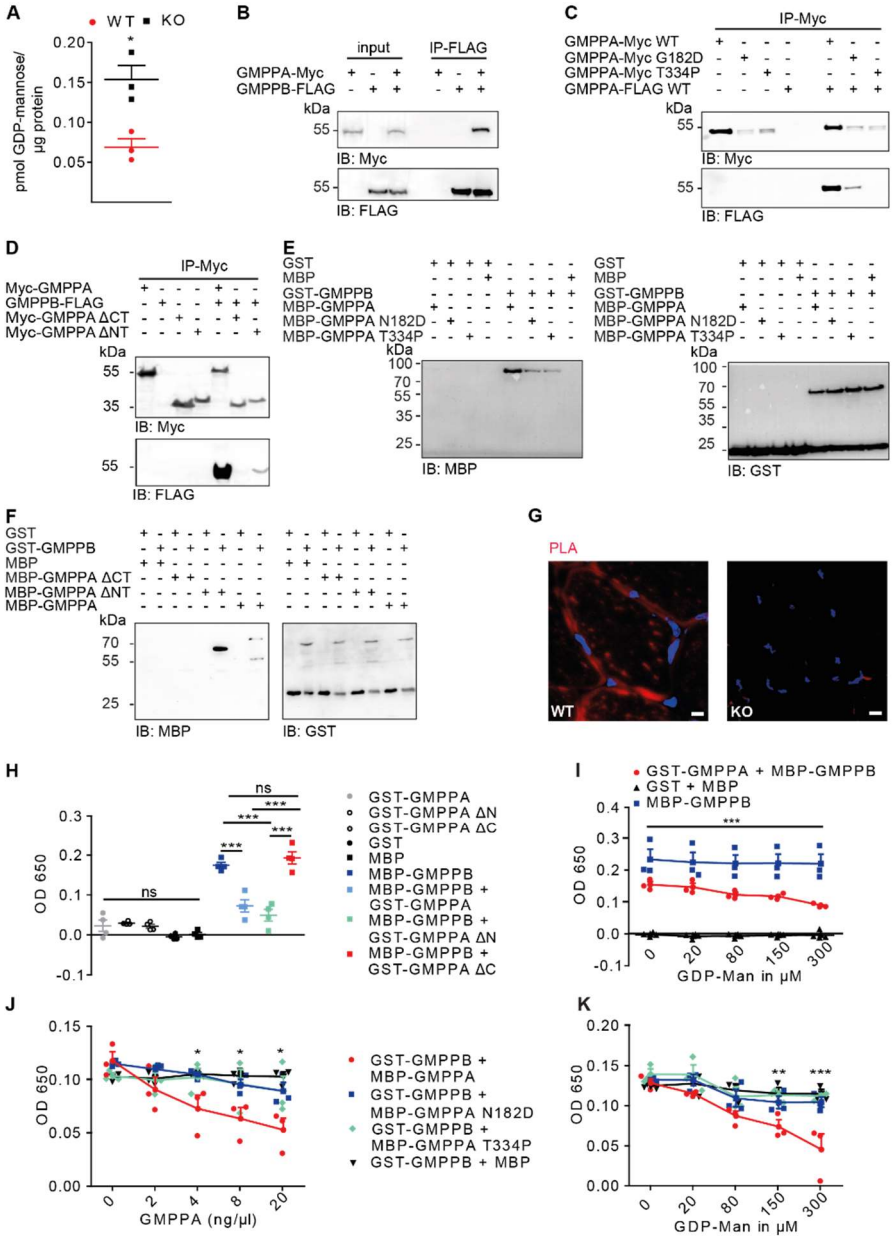

Figure 4. GMPPA is an allosteric inhibitor of GMPPB. A) GDP-mannose is increased in skeletal muscles of 8-month-old KO mice (n=3 mice per group; unpaired 2-tailed Student's t-test). **B)** Overexpressed GMPPA-Myc and GMPPB-FLAG co-precipitate (IP: Immunoprecipitation). **C)** Upon heterologous expression with GMPPB, the N-terminal GMPPA variant G182D is detected but not the C-terminal variant T334P. **D)** GMPPA devoid of the C-terminal aa 206-420 (ΔCT) does not interact with GMPPB, while GMPPA devoid of the N-terminal aa 1-205 (ΔNT) still co-precipitates with GMPPB. **E)** Pull-down of recombinant GST-GMPPA WT, -GMPPA N182D, -GMPPA T334P, and MBP-GMPPB. **F)** Pull-down of recombinant MBP-GMPPA deletion constructs and GST-GMPPB. **G)** Red signals indicate proximity of GMPPA and GMPPB of ≤40nm in WT but not in KO skeletal muscle in proximity ligation assays (PLA). Scale bars: 5µm. Additional controls are shown in Supplementary Figure 3. **H)** Recombinant purified MBP-GMPPB shows enzymatic activity, which is inhibited by an equal amount of recombinant GST-GMPPA in the presence of 80µM GDP-mannose (n=3 experiments; 1-way ANOVA with Bonferroni post-hoc test). **I)** Inhibition of GMPPB activity by GMPPA WT increases with higher GDP-mannose concentrations (n=3 experiments; 2-way ANOVA with Bonferroni post-hoc test). Controls are shown in Supplementary Figure 3. **J)** The enzymatic activity of recombinant GMPPB (20 ng/µl) is inhibited by increasing amounts of recombinant GMPPA WT but not by disease associated variants N182D and T334P (n=3 experiments; 2-way ANOVA with Bonferroni post-hoc test). **K)** The enzymatic activity of recombinant GMPPB is inhibited in a GDP-mannose dependent manner in the presence of recombinant GMPPA WT, but not in the presence of GMPPA N182D and T334P (n=3 experiments; 2-way ANOVA with Bonferroni post-hoc test). Quantitative data are presented as mean±SEM with individual data points.

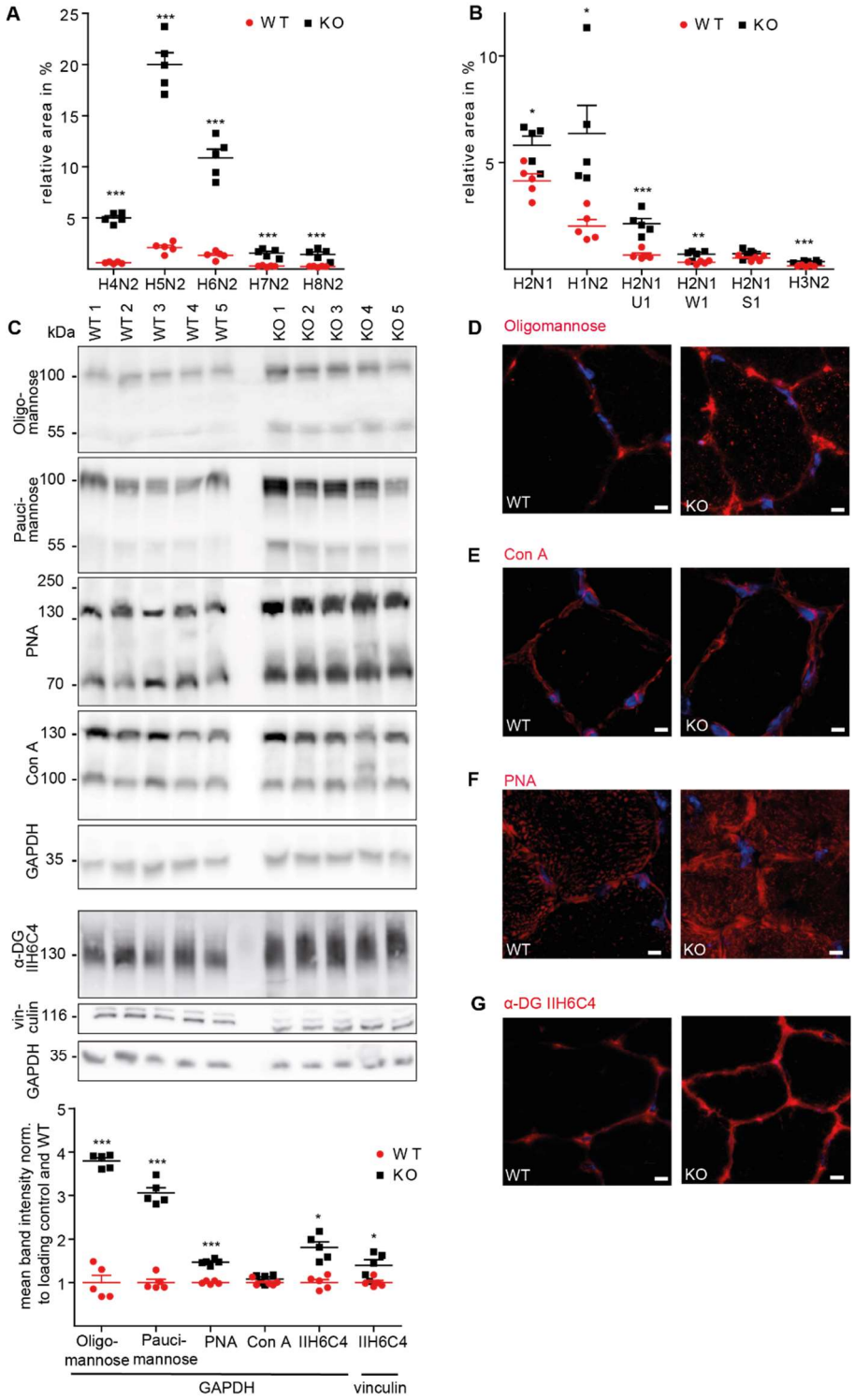

Figure 5. Loss of GMPPA causes α-DG hyperglycosylation. A,B) Skeletal muscle glycome analysis of 12-month-old fasted mice (n=5 per group; 1-way ANOVA with Bonferroni post-hoc test). Relative peak areas from MALDI-TOF spectra. A) *N*-glycans, B) *O*-glycans. H: hexose, N: N-acetylhexosamine. S: N-acetylneuraminic acid, U: glucuronic acid, W: glucuronic acid with one sulphate group. **C)** Immunoblot analyses of skeletal muscle lysates show increased signals for oligomannose, paucimannose, peanut agglutinin (PNA), and the glycosylation-specific α-DG epitope IIH6C4 in samples from 12-month-old KO mice. Signals for concanavalin A (Con A) are unchanged. Vinculin and GAPDH served as loading controls (n=5 mice per group; 2-way ANOVA with Bonferroni post-hoc test). **D-G)** Immunostainings of skeletal muscle sections from 12-month-old WT and KO mice (n=3 per group). Scale bars: 5 µm. Overviews and control stainings after PNGase F treatment are displayed in Supplementary Figure 4. **D)** Increased oligomannose signals in KO samples. **E)** Con A signals are unchanged. **F)** PNA signals are increased in KO samples. **G)** Signals for IIH6C4 are increased in KO samples. Quantitative data are presented as mean±SEM with individual data points.

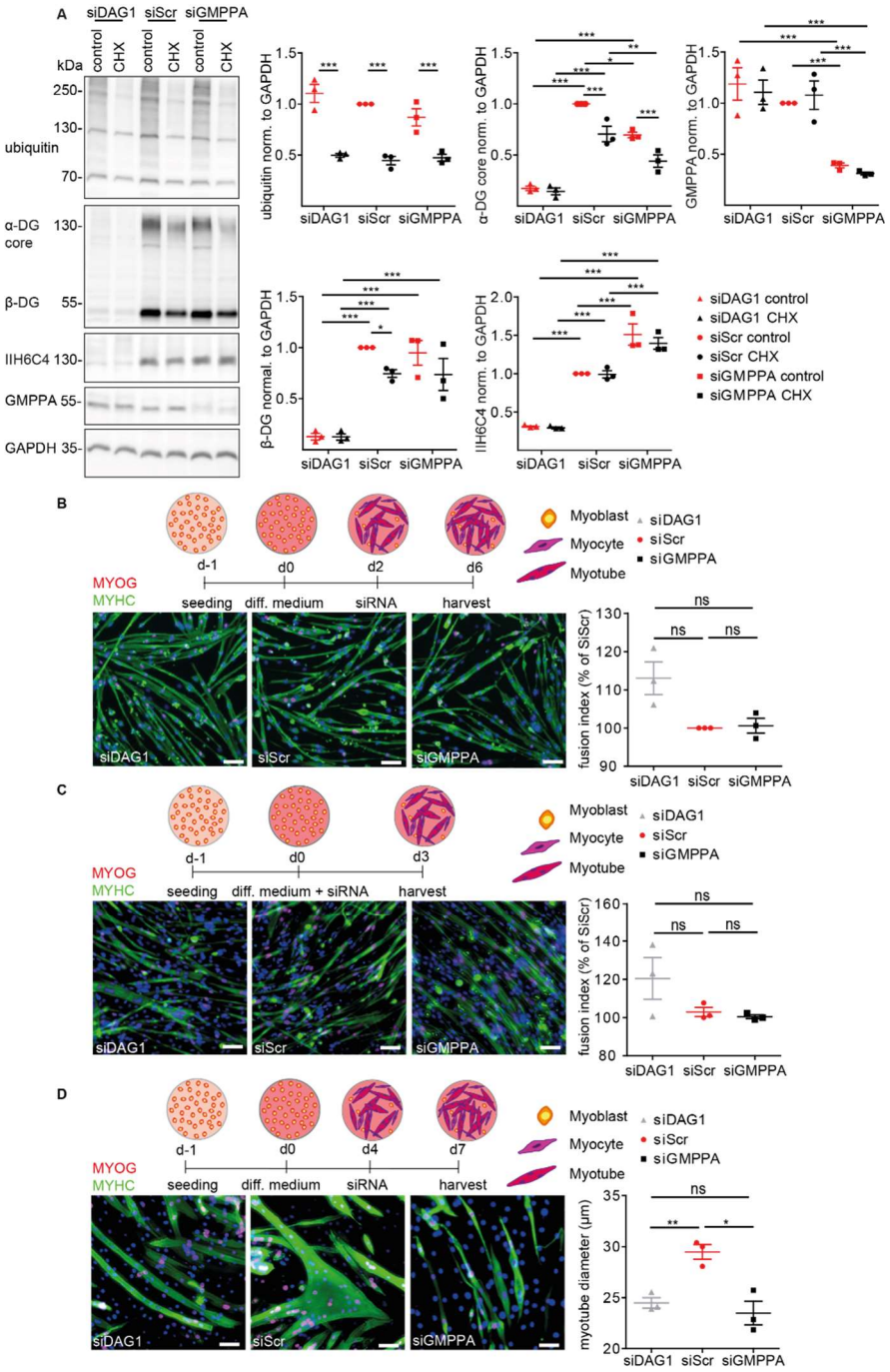

Figure 6. GMPPA knockdown in myoblasts increases α-DG turnover and causes myotube degeneration. A) Immunoblot analyses confirm efficient knockdown of either dystroglycan (siDag1) or GMPPA. Compared to controls (siScr) α-DG stability is decreased in the presence of cycloheximide (CHX) upon GMPPA knockdown. Ubiquitin served as a control for efficient CHX treatment. GAPDH served as loading control (n=3 experiments; 1-way ANOVA with Bonferroni post-hoc test). **B)** GMPPA knockdown does not affect the differentiation of primary myoblasts (n=3 experiments; 1-way ANOVA with Bonferroni post-hoc test). Experimental design, representative images of primary mouse myoblasts stained for myogenin (MYOG) or Myosin heavy chain (MYHC) and quantification of the fusion index. **C)** Knockdown of GMPPA does not affect the differentiation of the myoblast cell line C2C12 (n=3 experiments; 1-way ANOVA with Bonferroni post-hoc test). Experimental design, representative images stained for MYOG and MYHC and quantification of the myotube diameter. **D)** The size of C2C12 derived myotubes is altered upon knockdown of GMPPA (n=3 experiments; 1-way ANOVA with Bonferroni post-hoc test). Experimental design, representative images of differentiated C2C12 cells and quantification of myotube diameter. Nuclei are stained in blue. Scale bars B-D: 70µm. Quantitative data are presented as mean±SEM with individual data points.

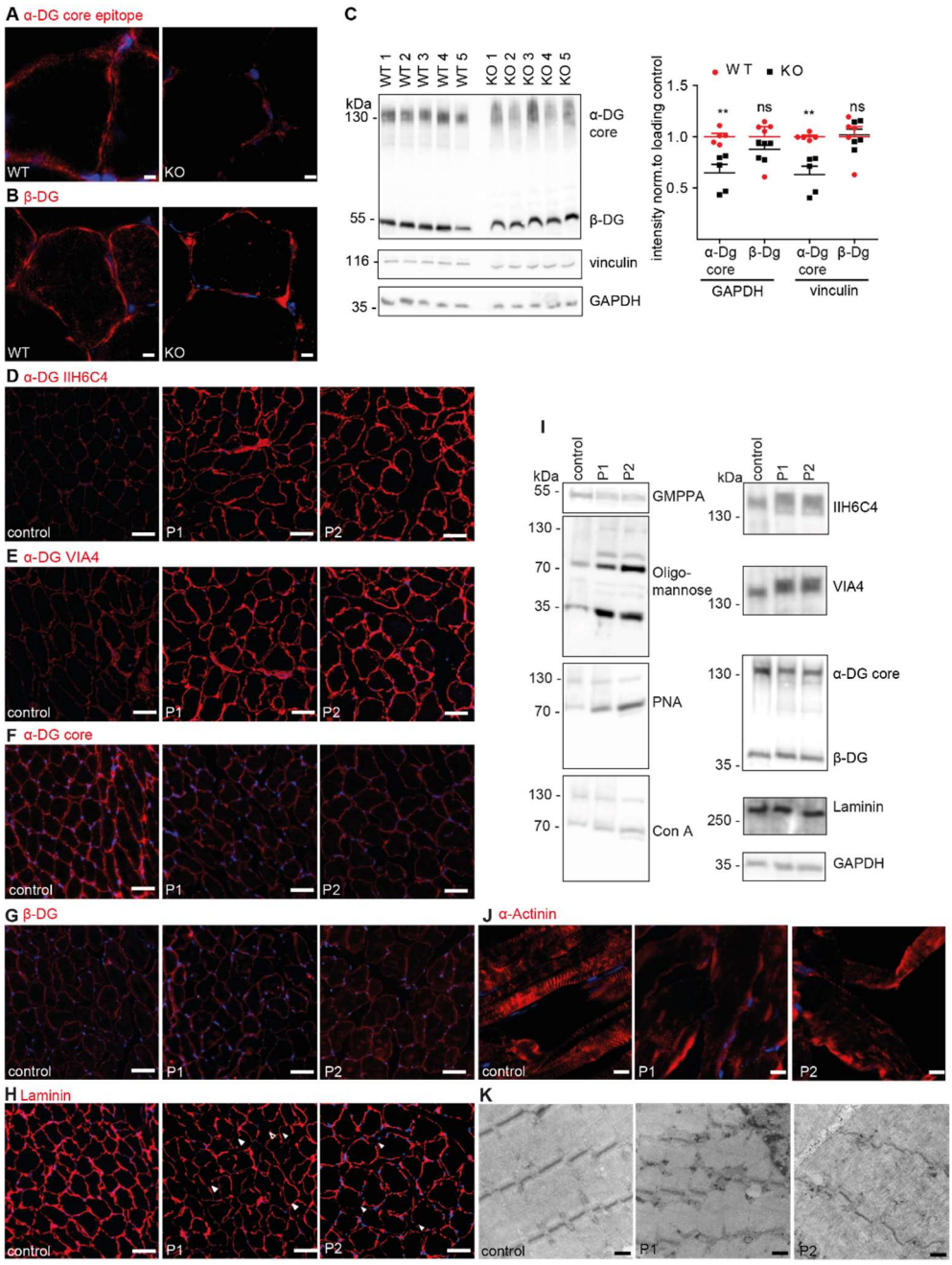

Figure 7. Hyperglycosylation and decreased abundance of α-DG in KO mice and in AAMR patients. A) Signals for the α-DG core are decreased in skeletal muscle sections of *Gmppa* KO mice at 12 months of age. Overviews and control stainings after deglycosylation with PNGase F are shown in Supplementary Figure 5. **B)** β-DG signals are unchanged. Scale bars A,B: 5µm. **C)** Skeletal muscle α-DG abundance is decreased in 12-month-old KO mice, while β-DG abundance is unchanged (n=5 per group; 2-way ANOVA with Bonferroni post-hoc test). Vinculin and GAPDH served as loading control. The quantification after enzymatic deglycosylation is shown in Supplementary Figure 5C. **D,E)** Immunostainings of cross sections of Musculus quadriceps femoris biopsies from patients (P1, P2) for the glycosylation-specific α-DG epitopes D) IIH6C4 and E) VIA4 show increased signal intensities compared to the control. **F)** Signal intensities for the α-DG core protein are decreased in patients. **G)** β-DG signal intensities are unchanged. **H)** In patients, laminin signals appear irregular (arrowheads). Scale bars D-H: 50µm. **I)** Immunoblot analyses of skeletal muscle lysates show decreased band intensities for GMPPA and the α-DG core in patient samples, while signals for oligomannose, PNA, and the glycosylation-specific α-DG epitope are increased. Note the shift of the bands for α-DG to a larger size in patients. The signals for Con A, β-DG and laminin are unchanged. GAPDH served as loading control. **J)** The regular α-actinin staining-pattern is almost absent in patient samples. Scale bars: 10µm. **K)** The ultrastructural analyses reveal disarranged myofibers and irregular Z-discs in patients. Scale bars: 500nm. Quantitative data are presented as mean±SEM with individual data points.

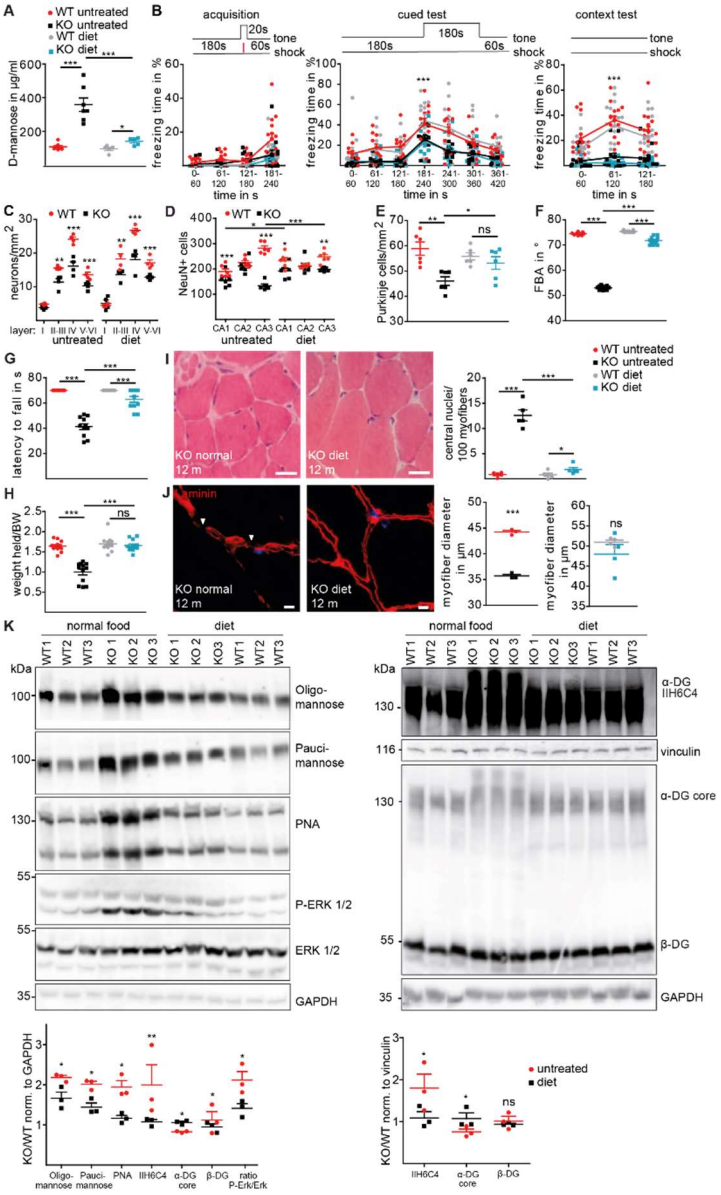

Figure 8. Motor impairments of *Gmppa* KO mice are largely prevented by dietary mannose depletion. A) Serum mannose almost normalizes upon dietary mannose-depletion (n=5-7 per group; 2-way ANOVA, Bonferroni post-hoc test). **B)** No improvement in the fear conditioning paradigm of 3-month-old KO mice on a mannose-depleted diet starting at postnatal day (P) 14 (n=12 per group; 2-way ANOVA, Bonferroni post-hoc test). **C)** Dietary intervention does not prevent abnormal cortical layering (n=4 per group; 2-way ANOVA, Bonferroni post-hoc test). **D,E)** Hippocampal neuron loss (D) and Purkinje cell loss (E) is attenuated by mannose restriction (n=6 per group; 2-way ANOVA, Bonferroni post-hoc test). **F)** The foot-base-angle (FBA) does not deteriorate in mannose-restricted KO mice (n=11 per group; 2-way ANOVA, Bonferroni post-hoc test). **G)** Almost normal latency to fall off an inverted screen in treated KO mice (n=11 per group; 2-way ANOVA,Bonferroni post-hoc test). **H)** The maximal weight held with fore-paws does not deteriorate in mannose-depleted KO mice (n=12 mice per group; 2-way ANOVA, Bonferroni post-hoc test). **I)** Dietary intervention normalizes skeletal muscle morphology. HE-stained sections of 12-month-old mice and quantification of centralized nuclei (n=12 mice per group; 2-way ANOVA, Bonferroni post-hoc test). Scale bars: 50µm. **J)** Treatment normalizes laminin distribution and myofiber diameter in KO mice (n=12 mice per group; unpaired 2-tailed Student´s t-test). Scale bars: 5µm. **K)** Immunoblot analyses of skeletal muscle lysates (white column: ratio WT/KO untreated mice, black column: ratio WT/KO treated mice; n=3 per group; 1-way ANOVA, Bonferroni post-hoc test). Signals for oligo- and paucimannose, PNA, glycosylation- and core-specific α-DG epitope, and P-ERK 1/2 normalize upon treatment. Beta-DG and BIP abundances are unchanged. Vinculin and GAPDH served as loading control. Statistical evaluation compares differences between genotypes in either the treated or untreated cohort or between both cohorts. Quantitative data are presented as mean±SEM with individual data points.